Hindawi Publishing Corporation
EURASIP Journal on Advances in Signal Processing
Volume 2010, Article ID 461538, 28 pages
doi:10.1155/2010/461538

Research Article

Tracking Algorithms for Multistatic Sonar Systems

Martina Daun[1] and Frank Ehlers[2]

[1] *Department of Sensor Data and Information Fusion (SDF), Fraunhofer FKIE, Neuenahrer Straße 20, 53343 Wachtberg, Germany*
[2] *NATO Undersea Research Centre (NURC), 19126 La Spezia, Italy*

Correspondence should be addressed to Frank Ehlers, frankehlers@ieee.org

Received 3 December 2009; Revised 5 May 2010; Accepted 23 June 2010

Academic Editor: Christoph F. Mecklenbräuker

Activated reconnaissance systems based on target illumination are of high importance for surveillance tasks where targets are nonemitting. Multistatic configurations, where multiple illuminators and multiple receivers are located separately, are of particular interest. The fusion of measurements is a prerequisite for extracting and maintaining target tracks. The inherent ambiguity of the data makes the use of adequate algorithms, such as multiple hypothesis tracking, inevitable. For their design, the understanding of the residual clutter, the sensor resolution and the characteristic impact of the propagation medium is important. This leads to precise sensor models, which are able to determine the performance of the surveillance team. Incorporating these models in multihypothesis tracking leads to a situationally aware data fusion and tracking algorithm. Various implementations of this algorithm are evaluated with the help of simulated and measured data sets. Incorporating model knowledge leads to increased performance, but only if the model is in line with the physical reality: we need to find a compromise between refined and robust tracking models. Furthermore, to implement the model, which is inherently nonlinear for multistatic sonar, approximations have to be made. When engineering the multistatic tracking system, sensitivity studies help to tune model assumptions and approximations.

1. Introduction

Submarines operate covertly, hidden under the surface of the sea. Maneuvering silently is their greatest threat. To detect a submarine, active sound is transmitted, which is then reflected by the submarine and recorded by a sensor. This is called active sonar. In active sonar, different types of signals are used: in particular, in this paper, we study frequency-modulated sweeps (FM), which provide a good-range resolution, and continuous wave signals (CW), which provide Doppler information. However, submarine designers build submarine hulls in shapes that give them stealth even for active sonar: in cases when just a single source and a single receiver are used, the submarine can minimize by clever navigation the presented target strength to disappear in the background. The background consists of noise and, which is even worse from a tracking point of view, of aspect-dependent reverberation. As a result, false alarms with geometry-dependent statistics occur. Consequently, an antistealth setup consists of multiple sources and receivers. This makes it almost impossible for the submarine to hide its strong echo returns. This concept is called multistatic active sonar. Covert receivers exploit the operational benefit that the submarine cannot determine whether it is detected or not. Exploiting the full multistatic setup will therefore result in additional detection probabilities.

The aim of target tracking is to determine the conditional probability of the target state given the measurement history of all data generated by the available multistatic source receiver pairs and, therein, from the available "signal channels" (FM or CW). A theoretically optimal approach for this tracking and fusion exists in the Bayesian framework [1]. For practical considerations, and to result in a real-time-capable algorithm, we applied specific techniques (adopted from ground moving target indication [2]) and evaluated their performance with the help of data sets from real measurements at sea and with simulated data sets.

By sequentially combining (via target tracking) all data, the multistatic setup provides the estimation of target location. However, to fuse data from different source and receiver

(S/R) pairs, a correct association between the receivers' data and all sound-reflecting objects is necessary. In the noisy and reverberant ocean environment, finding the true data associations is impeded by false alarms and missed detections. Even harder, the ocean only provides a fading channel for sound transmissions. Furthermore, the accuracy of measured contact and environmental data is limited by the given variability of the underwater sound channel and by budget or feasibility constraints on the quality and number of measurements.

Sonar performance modelling is able to describe the stochastic effects in the multistatic measurement. Together with a precise modelling of geometrical and kinematical features [3], a sensor model is constructed that becomes part of a sequential tracking algorithm, in this paper, it is the multihypothesis tracking (MHT) algorithm. Only the correct modelling allows a successful multisensor data fusion and by this the full exploitation of the multistatic sonar setup.

The MHT algorithm has a Kalman filter kernel. Because the sensor model is nonlinear, approximations are necessary and can be implemented in four different ways: linear transformation of each measurement in Cartesian coordinates with tracking in the Cartesian system (Cartesian L), unscented transformation (UT) [4] of each measurement in Cartesian coordinates with tracking in the Cartesian system (Cartesian UT), extended Kalman filtering (EKF) [5], and unscented Kalman filtering (UKF) [4].

The novel contribution of the paper is a precise and "situationally aware" fusion strategy for multistatic measurements inside the MHT framework.

Key prerequisites to achieve this are

(i) a precise modelling of the deterministic features in a multistatic measurement and incorporation of this measurement modelling in the framework of the Unscented Kalman Filter (Section 3) and

(ii) an optimal data fusion which can be found by weighting the fusion input by its quality. Quality is evaluated by solving the sonar equation for each source-receiver geometry, each ping, and each hypothetic target. The performance of the adaptive scheme is compared to static fusion schemes. Details are provided in Section 7.

Furthermore, we are applying

(i) for bistatic measurements an extension to the linearization methods in [6] a strategy to incorporate probabilistic features based on the Unscented Transformation. Additionally strategies based on the idea of UKF and EKF are developed in Section 6. The performance of the resulting four tracking architectures (Cartesian L, Cartesian UT, EKF, and UKF) is evaluated with the help of Monte Carlo simulations in Section 8.2

(ii) an algorithm for ground moving target indication to fuse contacts with additional Doppler information (Section 7.4).

The remainder of this paper is organized as follows. In Section 2, we describe the multistatic sonar system. In Sections 3 and 4, we model deterministic and probabilistic features of the multistatic sonar measurements. We specify the structure of a sequential tracking algorithm in Section 5, in particular the multihypothesis tracking algorithm (MHT), and adapt it for its application to multistatic sonar data in Section 6. In Section 7, we address the problem of finding an adequate fusion architecture. Results with experimental and simulated data are provided in Section 8. We summarize our findings in Section 9.

2. Multistatic Sonar

Multistatic active sonar involves multiple entities transmitting signals and receiving echoes. Receivers can be kept covert if they are spatially separated from the transmitter. Of interest for this paper is a system setup that consists of fixed arrays (Figure 1). This is used to create a barrier against submarine entry. The major advantage of multistatic sonar system is that there are more "ears" in the water to improve the detection, localization and identification of undersea objects, which results in a reduced false alarm rate.

Today's submarines are designed to be stealthy. By clever navigation, they can avoid detection from a monostatic active sonar. But a multistatic system has additional detection opportunities in comparison to a monostatic system. To exploit this benefit, the data gathered at different transmitter-receiver pairs must be associated. In other words, data fusion has to find the best combination out of all possible detections from all source-receiver pairs in a series of measurements. Sonar performance prediction modelling shows that only rarely two distributed sensors have a similar quality on a specific ping of the target track. Therefore, data fusion algorithms must be based on realistic modelling of sensor performance for each sensor, each ping, and each target. Data are weighted so that data, which are considered more accurate or valid, are given more weight in the algorithms. This is implementing a "situationally aware" tracking, which has an improved performance compared to architectures of tracking algorithms with fixed sensor performance setting.

In practice, the software system for multistatic active sonar involves three steps.

(1) The collation of contact files from the networked receiving buoys: there is a contact file for each ping (i.e., transmission of an acoustic signal and each receiver). Each contact file contains for each detected echo the measurement vector (depending on the associated CW/FM channel)

$$\mathbf{z}^{\mathrm{CW}} = (\varphi, \tau, \dot{r})^T, \qquad \mathbf{z}^{\mathrm{FM}} = (\varphi, \tau)^T, \tag{1}$$

where τ is the time of arrival, which is the bistatic range r divided by the speed of sound, $\dot{r}$ is the bistatic range-rate, which is proportional to the Doppler, and φ is the azimuth measurement. For each contact the associated SNR-value is also stored.

Please note that we assume a constant speed of sound over range r. The formula can be extended to other functional relationships in case that this relationship

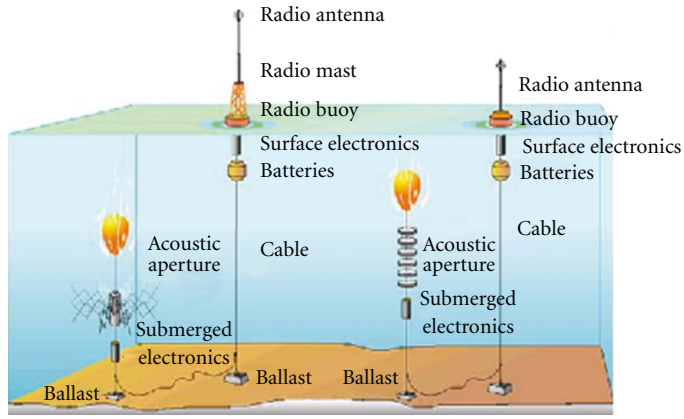

(a) DEMUS system

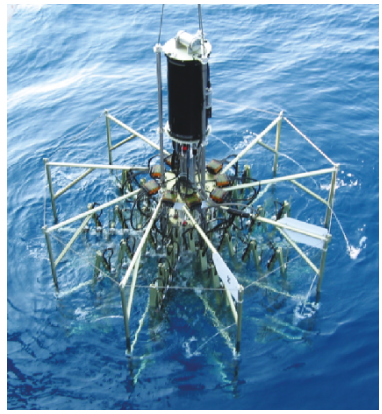

(b) Stationary receiver

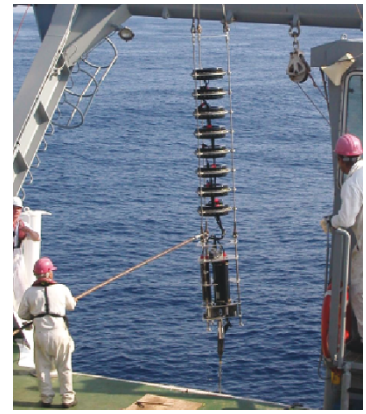

(c) Stationary acoustic source

FIGURE 1: Illustration of a stationary multistatic sonar system (a). A prototype of a stationary receiving system is shown in (b). As an acoustic source, the stationary system shown in (c) has been used. The system with three receivers and the source is called DEMUS. See [7, 8] for further information.

is a priori known and that there is evidence that this will improve the localization accuracy.

(2) The use of data fusion and tracking algorithms to combine the information in the contact files. This is the topic of this paper.

(3) The output of the algorithm into a human computer interface that can facilitate interpretation of the data. The output consists of a set of tracks that is updated in real-time as a new contact file is received. Each track must include the position, speed, and course of the target. This information is stored in the state vector $\mathbf{x}$.

3. Modelling Deterministic Features of Multistatic Sonar

Let $\mathbf{q} = (x, y)^T$ be the target position and $\mathbf{s} = (s_x, s_y)^T$ and $\mathbf{o} = (o_x, o_y)^T$ the position of the source, and the receiver, respectively. The receiver orientation (heading) is given by ϑ, c.f. Figure 2. Then, the measurements can be expressed as

$$\begin{aligned} \varphi &= \arctan\left(\frac{x - o_x}{y - o_y}\right) - \vartheta, \\ \tau &= \frac{(|\mathbf{q} - \mathbf{s}| + |\mathbf{q} - \mathbf{o}|)}{c_S}, \\ \dot{r} &= \frac{\partial \tau}{\partial t} c_S, \end{aligned} \tag{2}$$

where $|\cdots|$ denotes the Euclidian norm and c_S is the propagation speed of sound in water.

3.1. Timing. Assuming the target velocity to be constant between two consecutive pings, the standard bistatic range measurement equation (2) (where $r = \tau \cdot c_S$) is replaced by

$$r = |\mathbf{q} + t_0\dot{\mathbf{q}} - \mathbf{s}| + |\mathbf{q} + t_0\dot{\mathbf{q}} - \mathbf{o}|, \tag{3}$$

where t_0 is the travelling time of the sound from the source to the target. Let c_S denote the propagation speed of the signal,

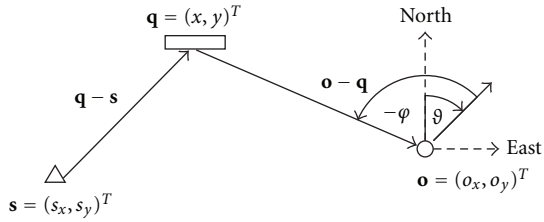

Figure 2: Bistatic setup; sound from source at s is reflected by the target at q and received at o. ϑ is the heading of the receiver relative to North.

then we need to solve $\sqrt{(x + t_0\dot{x} - s_x)^2 + (y - t_0\dot{y} - s_y)^2} = t_0 c_S$. Calculations yield

$$t_0 = \frac{(\mathbf{q}-\mathbf{s})^T\dot{\mathbf{q}}}{(c_S^2 - v_T^2)} + \sqrt{\frac{\left((\mathbf{q}-\mathbf{s})^T\dot{\mathbf{q}}\right)^2}{(c_S^2 - v_T^2)^2} + \frac{|\mathbf{q}-\mathbf{s}|^2}{c_S^2 - v_T^2}}, \quad (4)$$

with $v_T = |\dot{\mathbf{q}}|$.

3.2. Range-Doppler Ambiguity. Relative movement between source, target, and receiver leads to frequency shifts Δf in the received target echo. For FM signals, the matched filter converts these frequency shifts into shifts of detection time. Assuming perfect knowledge of the relative movement, these shifts can be corrected. The frequency characteristics $f_{\min} + t(f_{\max} - f_{\min})/\Delta_S = f_{\min} + \Delta f$ delivers the time shift $t = \Delta f \Delta_S/(f_{\max} - f_{\min})$, where Δ_S is the duration of the signal. The modified measurement equation for range is therefore given by

$$r = |\mathbf{q}-\mathbf{s}| + |\mathbf{q}-\mathbf{r}| + \frac{\dot{r}}{2}\frac{f_{\max}+f_{\min}}{f_{\max}-f_{\min}}\,\Delta_S, \quad (5)$$

where the bistatic range-rate $\dot{r}$ is given by

$$\dot{r} = \frac{(\mathbf{q}-\mathbf{s})^T(\dot{\mathbf{q}}-\dot{\mathbf{s}})}{|\mathbf{q}-\mathbf{s}|} + \frac{(\mathbf{q}-\mathbf{o})^T(\dot{\mathbf{q}}-\dot{\mathbf{o}})}{|\mathbf{q}-\mathbf{o}|}. \quad (6)$$

Thus, the measurement equation is corrected by the estimated Doppler value (calculated from the estimated target position and velocity).

Remarks. The speed of sound waves is slow compared to electromagnetic waves. Therefore, a precise modelling of geometric features and Doppler effects is important. Without this precise modelling geometry-dependent errors estimating, the target state hampers the correct contact association and finally the optimal exploitation of the multistatic data fusion.

Of course, correction for both features (timing and range-Doppler ambiguity) can be done simultaneously. The combined range equation is

$$r = |\mathbf{q} + t_0\dot{\mathbf{q}} - \mathbf{s}| + |\mathbf{q} + t_0\dot{\mathbf{q}} - \mathbf{o}| + \frac{\dot{r}}{2}\frac{f_{\max}+f_{\min}}{f_{\max}-f_{\min}}\,\Delta_S, \quad (7)$$

For further reference in this paper, an algorithm implementing equation (4) is called "TiCor", (5) is "DoCor", and (6) is "DoTiCor". Note that in (4), (5), and (6), the range is a function of the target velocity.

Table 1: Probabilistic features in the underwater sound channel.

Probabilistic features in the underwater sound channel are
(1) floating, drifting, or rotating sensor platforms;
(2) rapidly changing (spatially and temporally) environmental conditions;
(3) multipath arrivals with very variable structure;
(4) high noise levels at sensors; (e.g., on towed array due to flow noise or on stationary systems due to passing vessels);
(5) strong fading;
(6) for active sonar a highly cluttered and aspect-dependent reverberation background.

4. Modelling Probabilistic Features of Multistatic Sonar

Probabilistic features in the underwater sound channel must be reflected in the tracking algorithm. Table 1 lists the probabilistic features influencing the sonar measurement.

4.1. Mapping of Uncertainties in the Measurements to Cartesian Coordinates. The effect of items (1) to (2) in Table 1 is that only estimates for sound speed c_S, receiver **o,** and source **s** positions as well as receiver orientation (heading) ϑ are available.

Hence, we model the uncertainty following [9] by $\mathbf{o} \sim \mathcal{N}(\mathbf{o}; \overline{\mathbf{o}}, \mathbf{P_o})$, $\mathbf{s} \sim \mathcal{N}(\mathbf{s}; \overline{\mathbf{s}}, \mathbf{P_s})$, $c_S \sim \mathcal{N}(c_S; \overline{c}_S, \sigma_{C_S})$ and $\vartheta \sim \mathcal{N}(\vartheta; \overline{\vartheta}, \sigma_\vartheta)$.

The effect of items (3) and (4) in Table 1 is that the receiving time $\overline{\tau}$ and receiving bearing $\overline{\varphi}$ are only estimates of the true values τ and φ, respectively

$$\tau \sim \mathcal{N}(\tau; \overline{\tau}, \sigma_\tau), \qquad \varphi \sim \mathcal{N}\left(\varphi; \overline{\varphi}, \sigma_\varphi\right). \quad (8)$$

We assume φ to be Gaussian distributed because this is an appropriate model for our measurement equipment. An error in the receiver heading can be incorporated by enlarging the error in azimuth information; that is, $\sigma_{\hat{\varphi}} = \sqrt{\sigma_\varphi^2 + \sigma_\vartheta^2}$. Without loss of generality, we set the expected receiver heading to 0° in this paper.

This results in a new definition of an artificial measurement vector

$$\mathbf{z}^{(a)} = \left(\varphi, \tau, c_S, \mathbf{s}^T, \mathbf{o}^T\right) = \left(\left(\mathbf{z}^{\mathrm{FM}}\right)^T, c_S, \mathbf{s}^T, \mathbf{o}^T\right). \quad (9)$$

From this, the 2D-target position $\mathbf{q} = (x, y)^T$ can be estimated according to

$$\mathbf{q} = g(\mathbf{z}(a)), \quad (10)$$

where the functional relationship in g is given by the formulas (for derivation, see e.g. [10]):

$$x = \sin(\varphi)\cdot\gamma + o_x, \qquad y = \cos(\varphi)\cdot\gamma + o_y, \quad (11)$$

where $\alpha = \arctan(s_x - o_x/s_y - o_y) - \varphi$, $\delta = \sqrt{(s_x - o_x)^2 + (s_y - o_y)^2}$, and $\gamma = ((r \cdot c_S)^2 - \delta^2)/2(r \cdot c_S - \delta\cos(\alpha))$.

To approximate the probability density function (pdf) of $\mathbf{q}$ we can utilize the known pdf of $\mathbf{z}_a$ and the functional relationship described by g. In [6], a linearization approach has been presented to derive the Cartesian covariance matrix: g is approximated by linearizing. In Section 6.2, we derive an alternative approach based on the unscented transform (UT) [4] that uses an approximation of the probability density function (pdf) instead of an approximation of the nonlinear transformation from measurements and environmental parameters to Cartesian coordinates. We compare the performance of the different approaches in Section 8.2.1.

Uncertainties related with Doppler measurements will be addressed in Section 7.4.

4.2. Association. Following the discussion in Section 4.1 , for each source/receiver pair alone there remains uncertainty about the target's location after the measurement of τ and φ. The strength of multistatic data fusion is to exploit the inputs from (at least two) source receiver geometries to estimate the targets true position with a higher accuracy, using a kind of triangulation technique by overlaying the uncertain position measurements available. A prerequisite for this triangulation is an unbiased estimation and correctly modelled uncertainties. The difficulty is sketched in Figure 3. Measurements of the same target (star), but corresponding with different illuminator and receiver configurations, are illustrated by their mean (circles) and covariances (ellipses). If the estimate is biased or has an undersized covariance, Figure 3(a), this may prevent the algorithm from correctly associating measurements of different source-receiver pairs to the same target. For correct measurement modelling, Figure 3(b), the target can precisely be located in the intersection area of the ellipses.

Additionally, due to item (4) in Table 1 and (even worse because of aspect dependency) due to item (6), not only are target echoes fed into the data fusion, but also false alarms. This results in multiple hypotheses for triangulation crossing points, and the correct association between target and received echoes has to be made. This is why estimation errors should not be modelled too pessimistically, since this would lead to too many crossing possibilities.

Again due to items (4) and (6) (Table 1), the detector (i.e., the software that generates contact data) cannot analyze all parts of the signal: A kind of decision threshold has to be defined to set the performance of a specific sensor following its receivers operating characteristics (ROC). This defines the probability of detection (P_D) and probability of false alarms (ρ_F) that has to be expected from this sensor. Since echoes from the target can be missed, the probability for this hypothesis has to be taken into account within all following data fusion and processing steps. Item (5) is increasing this difficulty: due to fading channels, even for a high false alarm setting it is not guaranteed that the target echo has generated a contact.

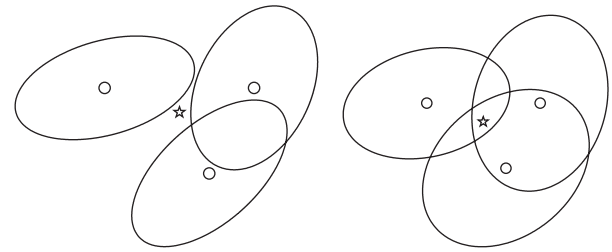

(a) inaccurate measurement description: multisensor association fails

(b) correct measurement description: the target can be located in the intersection area of the ellipses

Figure 3: Visualisation of *multi*sensor fusion. The measurement information of three S/R pairs is visualized by ellipses. The true target location is shown as a star.

Correct modelling of these probabilistic effects for each single bistatic source and receiver combination is the prerequisite of multisensor fusion. In the next section, we will show, how it can be handled within the scheme of automatic sequential tracking techniques.

5. Automatic Sequential Tracking Techniques

Bayesian target tracking is iterative updating of conditional probability densities of the target state $\mathbf{x}_k$ (containing the target components that are to be estimated, for example, the target position and velocity) at time t_k given all accumulated sensor data $Z^k = \{Z_1, \ldots, Z_k\}$, where $Z_k = \{z_k^{(1)}, \ldots, z_k^{(n_k)}\}$ denotes the set of n_k measurements collected at time t_k. It exploits all available a priori information on the target dynamics and the sensor performance in terms of statistical models. Each update consists of a prediction, which is determined by the target dynamics model. The prediction is followed by a filtering step, which exploits the current sensor data and the sensor model. The sensor data at each scan k, as well as the sensor model, are the constituents of the likelihood function. According to Bayes' rule, the conditional density at time t_k, given all sensor data up to and including time t_k can be sequentially calculated, that is

$$p\left(\mathbf{x}_k \mid Z^k\right) = p\left(\mathbf{x}_k \mid Z_k, Z^{k-1}\right) \propto p(Z_k \mid \mathbf{x}_k)\, p\left(\mathbf{x}_k \mid Z^{k-1}\right), \tag{12}$$

can be derived from the densities optimal estimators according to particular cost functions. The likelihood function $p(Z_k \mid \mathbf{x}_k)$ can be understood as a weighting function, scoring possible target states by the new incoming data. The likelihood reflects the match of measurement and target state, additionally it depends on the sensor performance. Thus, let e_k denote the event of target detection by one of the measurements in Z_k and $\bar{e}_k$ be the event that the target was missed, then the single target likelihood function can be separated in two summands

$$p(Z_k \mid \mathbf{x}_k) = p(Z_k, e_k \mid \mathbf{x}_k) + p(Z_k, \bar{e}_k \mid \mathbf{x}_k), \tag{13}$$

with

$$p(Z_k, e_k \mid \mathbf{x}_k) = p(e_k \mid \mathbf{x}_k)p(Z_k \mid \mathbf{x}_k, e_k)$$
$$= p(e_k \mid \mathbf{x}_k)p_{\mathrm{FA}}(n_k - 1)\rho_{\mathrm{F}}^{n_k-1}\sum_{i=1}^{n_k} p\left(z^{(i)} \mid \mathbf{x}_k, e_k^i\right), \quad (14)$$

where e_k^i represents the interpretation that the target was detected by measurement $\mathbf{z}_k^{(i)}$ and all measurements $\mathbf{z}_k^{(j)}$ with $j \neq i$ are false alarms. Due to the assumption that the target is detected by one measurement at most, $p_{\mathrm{FA}}(n_k - 1)$ represents the probability of obtaining $n_k - 1$ false measurements and ρ_{F} is the false alarm density, that is, the probability of obtaining a false alarm at a specific position of the observation area. The second summand is

$$p(Z_k, \bar{e}_k \mid \mathbf{x}_k) = \left(1 - p(e_k \mid \mathbf{x}_k)\right) p_{\mathrm{FA}}(n_k)\rho_{\mathrm{F}}^{n_k}, \quad (15)$$

that is, all measurements are false.

5.1. Modelling Assumptions of Sequential Target Tracking. In the application of sequential target tracking, the likelihood function needs to be modelled appropriately: in this paper we assume uniformly distributed false alarms; that is, we choose a fixed value of ρ_{F}. Thus, the probability $p_{\mathrm{FA}}(n_k)$ required for (14) and (15) is calculated according to a Poisson distribution with parameter ρ_{F}, that is, $p_{\mathrm{FA}}(n_k) = e^{-\rho_{\mathrm{F}}}(\rho_{\mathrm{F}}^{n_k}/n_k!)$. The probability of detection $p(e_k \mid \mathbf{x}_k)$ is further replaced by some fixed value P_{D}. According to these assumptions, the likelihood function can be calculated. But, obviously, the choice of the parameters P_{D} and ρ_{F} will have a significant influence on the tracking process. These assumptions on the probability of detection and false alarms are typical for many tracking applications, see for example [1, 11]. We will use this by default in our tracking algorithm. In Section 7, we discuss the consequences of the assumption of a fixed P_{D} in the multistatic scenario in more detail and present an approach to mitigate this constraint.

The target motion model is describing the evolution of the target state over time and needs to be defined in the tracking algorithm. We use the nearly constant velocity model that describes evolution by a linear transformation $\mathbf{F}_{k+1|k}$ plus a noise term $\mathbf{G}_{k+1|k}\mathbf{v}_{k+1}$ which is modelling the uncertainty about the targets next movement, that is,

$$\mathbf{x}_k = \left(\mathbf{q}_k, \dot{\mathbf{q}}_k\right)^T, \quad \text{with } \mathbf{q}_k = (x, y)^T \text{ and } \dot{\mathbf{q}}_k = (\dot{x}, \dot{y})^T \quad (16)$$

$$\mathbf{x}_{k+1} = \mathbf{F}_{k+1|k}\mathbf{x}_k + \mathbf{G}_{k+1|k}\mathbf{v}_{k+1}, \quad (17)$$

where $\mathbf{F}_{k+1|k}$ and $\mathbf{G}_{k+1|k}$ are matrices and $\mathbf{v}_{k+1}$ is a Gaussian process noise, see [12, 13].

5.2. Data Association and Tracking with Multihypothesis Tracking (MHT). In this section, an implementation of automatic sequential tracking is described. The implemented technique is called multihypothesis tracking (MHT). We follow the MHT architecture as described in [13], which will allow us to leverage on it successful application for ground moving target tracking. This section contains only an outline of the implemented MHT, for more details we refer to [13]:

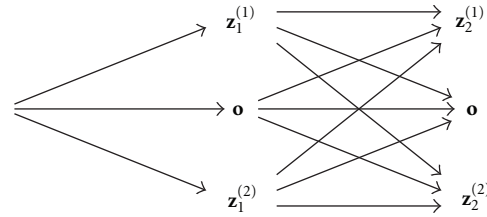

Figure 4: Hypothesis generation: In every time scan, the number of hypotheses increases by the factor $m_k + 1$ (number of measurements plus event of missed detection). A missed detection is illustrated by a circle.

The key idea of MHT is to describe the conditional probability density given in (12) by a Gaussian mixture. Therefore, a hypothesis tree is generated starting from an appropriate initialisation. Every new incoming measurement induces a new hypothesis. As a simple example, we consider a scenario with two measurements at time t_1, and also at time t_2. After time t_1 the MHT consists of three hypotheses, either $\mathbf{z}_1^{(1)}$ belongs to the target, or $\mathbf{z}_1^{(2)}$, or the target has not been detected. After time t_2, the number of hypotheses has increased to 9, as in every time scan the number of hypotheses increases by the factor $m_k + 1$.

A hypothesis within the MHT tree reflects a specific association possibility and can be represented by an expectation, $\mathbf{x}_{k+1|k+1}^{(i)}$, and a covariance matrix, $\mathbf{P}_{k+1|k+1}^{(i)}$ (describing a Gaussian density). Additionally, a hypothesis corresponds with a respective weight $p^{(i)}$ that is sequentially updated (Figure 5) and initialized by $p^{(0)} = 1$. For linear dependency of measurement and state vector, that is, $\mathbf{z}_k = \mathbf{H}\mathbf{x}_k$, the Kalman filter formulas can be applied for state estimation. The respective measurement update of each hypothesis is also given in Figure 5. Thus, the MHT consists of several Kalman filters running in parallel, such that its performance depends to a great extent on the performance of the Kalman Filter. For a nonlinear measurement equation (as in multistatic applications), appropriate approximation techniques must be applied. We address this topic in more detail in Section 6.2.

The MHT suffers from exponential growth of hypotheses, which raises the claim for appropriate hypotheses reduction techniques. We use hypotheses pruning (deleting hypotheses with low weights), hypotheses merging (combining similar hypotheses), and gating (considering reliable measurement to track combinations only) techniques to make it real-time capable. The more exact the modelling of the target dynamics and the measurement process the better these techniques work! The MHT algorithm as described above is a single target tracker, but it can easily be extended to handle multiple well-separated targets. This is implemented by a track management overarching the MHT structure: For each selected contact we start a tentative track and build up a hypothesis tree by exploiting the measurement information of following time scans. The track will be tested for belonging to a true target by calculating a likelihood ratio (LR) that

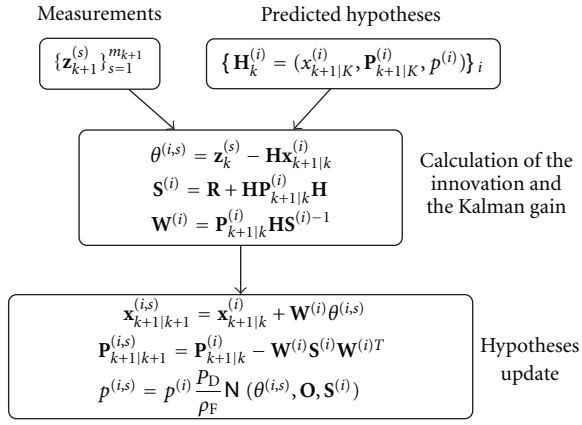

Figure 5: Measurement update step of the MHT: for each hypothesis $\mathbf{H}_k^{(i)}$ at time t_k and each measurement $\mathbf{z}_{k+1}^{(s)}$ a new hypothesis $\mathbf{H}_{k+1}^{(i)} = (\mathbf{x}_{k+1|k}^{(i)}, \mathbf{P}_{k+1|k}^{(i)}, p^{(i)})$ is generated.

is equal to the sum of hypotheses weights, [13]. Thus, by choosing appropriate thresholds A and B a track is extracted if the LR exceeds the threshold A and is terminated if it falls below B. Gating methods ensure individual processing of well separated targets.

Figure 6 illustrates one cycle of the MHT for a single track, it consists of the following steps:

(i) prediction of the current hypothesis tree according to the assumptions on target motion,

(ii) generation of new hypotheses according to the latest measurement information (measurement update, see Figure 5) and including the possibility of missing detections,

(iii) hypotheses tree reduction techniques,

(iv) evaluation of tracks (confirmation or deletion).

Further instances of track management are track merging and track splitting [13].

6. Approximation Techniques to Apply Sequential Tracking Techniques to Multistatic Sonar

By applying the sequential tracking technique, the multistatic measurement is split into bistatic measurements which are fed one by one into the tracking algorithms.

6.1. Handling Large Number of Contacts. For active sonar, as described in Section 2, the target strength of a submarine is designed to be small. As also described in Section 2, the application of active sonar in shallow water produces a large number of false alarms. Using all these contacts would stress the MHT structure and would cause an intractable size of the hypothesis tree. On the other hand, due to the multiple aspects of the target in multistatics, there is a high probability for a strong echo of at least one of the receivers. We are making use of this implicitly by defining an initial threshold (IT) with contacts whose SNR-value has to cross in order to initiate a new track. The detection threshold (DT) is used for updating existing hypotheses, allowing high accuracy maintenance of the track. The detection threshold (DT) is used for updating existing hypotheses. DT is lower than IT allowing for as many cross-fixing opportunities with contacts from different S/R as possible in order to maintain high accuracy of the target state estimation inside the track.

6.2. Handling Nonlinearities in Target Tracking for Bistatic Sonar. In the application of monostatic and bistatic sonar, the measurements are nonlinear functions of the target state $\mathbf{x}_k$ and the environmental parameters $\mathbf{a} = (c_S, \mathbf{o}^T, \mathbf{s}^T)$. Ignoring noise effects, the measurement vector $\mathbf{z}_k$ (either $\mathbf{z}_k^{\mathrm{FM}}$ or $\mathbf{z}_k^{\mathrm{CW}}$) can be described by a nonlinear function

$$\mathbf{z}_k = h(\mathbf{x}_k, \mathbf{a}). \tag{18}$$

The functional relationship in h is directly related to the function $g(\mathbf{z}_k^{\mathrm{FM}}, \mathbf{a}) = \mathbf{q}$ (defined in Section 3). Note that h is not invertible since the dimension of $\mathbf{x}_k$ and $\mathbf{a}$ is larger than the dimension of $\mathbf{z}_k$. Thus, h as well as g presume knowledge of $\mathbf{a}$.

Several approximation techniques like the EKF [5] and UKF [4] exist and fit perfectly in the framework of the MHT: only the measurement update component (see Figure 5) of the MHT is affected.

To concentrate on the measurement update and to ignore influences of the MHT approximations, we look in this section at a simplified scenario of one target, one source receiver pair and no missed detections and false alarms. Thus, the MHT structure reduces to a simple Kalman filter that consists of two steps: Prediction of the track state (usually in Cartesian coordinates) and track update using the measurement information. Two different ways to handle the nonlinear measurement equation in these schemes are investigated:

(i) the measurement is transformed into Cartesian coordinates and the Kalman Filter updates the target state in Cartesian coordinates (resulting in two algorithms: Cartesian L and Cartesian UT, resp.);

(ii) the predicted state is transformed into the measurement space to perform the filter update (which is the method used in UKF and EKF algorithms).

Figure 7 illustrates these two approaches.

The application of the Cartesian Kalman Filter works in a straightforward way by exploiting the transformation described in Section 4.1. Instead, the standard UKF and EKF need to be adapted to account for the uncertainties in the environmental parameters. As in Section 4.1, we assume the heading vector to be zero and pick up the uncertainty in the azimuth uncertainty.

6.3. Handling A Priori Information. The aim of target tracking (c.f. Section 5) is to determine the conditional probability

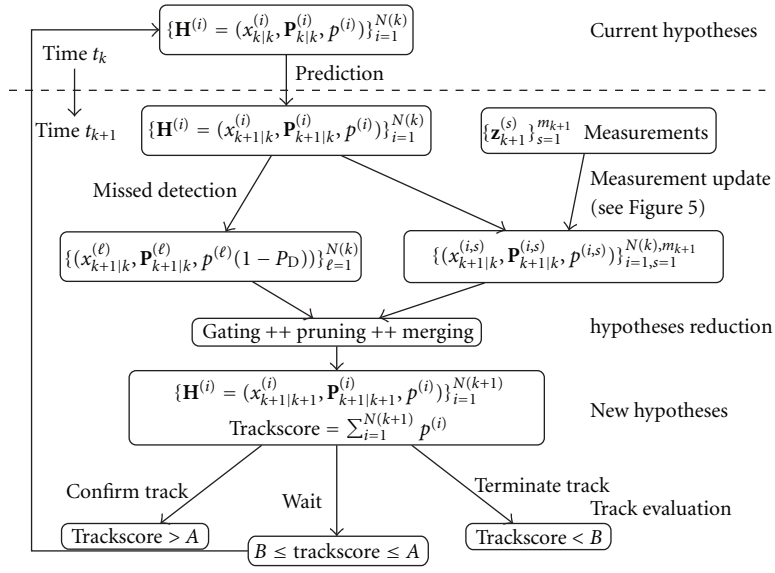

Figure 6: One cycle of the MHT: prediction of hypotheses; update of hypotheses; hypotheses reduction (by gating, pruning, and merging); track confirmation or deletion.

of the target state $\mathbf{x}_k$ at time t_k given the measurement history, $\mathbf{Z}^k = \{\mathbf{z}_1, \ldots, \mathbf{z}_k\}$, and all available a priori information, here $\bar{\mathbf{a}} \sim \mathcal{N}(\bar{\mathbf{a}}; \mathbf{a}, \mathbf{C}_a)$, where $\bar{\mathbf{a}}$ describes the assumed values and $\mathbf{a}$ the unknown, but true parameters:

$$
\begin{aligned}
p\left(\mathbf{x}_k \mid \mathbf{Z}^k, \bar{\mathbf{a}}\right) &= \int p\left(\mathbf{x}_k, \mathbf{a} \mid \mathbf{Z}^{k-1}, \mathbf{z}_k, \bar{\mathbf{a}}\right) \mathrm{d}\mathbf{a} \\
&= \int \frac{p\left(\mathbf{z}_k \mid \mathbf{x}_k, \mathbf{a}, \mathbf{Z}^{k-1}, \bar{\mathbf{a}}\right) p\left(\mathbf{x}_k, \mathbf{a} \mid \mathbf{Z}^{k-1}, \bar{\mathbf{a}}\right)}{\int p(\mathbf{z}_k \mid \mathbf{x}_k, \mathbf{a}) p(\mathbf{x}_k, \mathbf{a} \mid \mathbf{Z}^{k-1}, \bar{\mathbf{a}}) \mathrm{d}(\mathbf{x}_k, \mathbf{a})} \mathrm{d}\mathbf{a} \\
&= \int \frac{\mathcal{N}\left(\mathbf{z}_k; h\left(\mathbf{x}_k^{(a)}\right), \mathbf{R}\right) \mathcal{N}\left(\mathbf{x}_k^{(\mathbf{a})}; \mathbf{x}_{k|k-1}^{(\mathbf{a})}, \mathbf{P}_{k|k-1}^{(\mathbf{a})}\right)}{\int \mathcal{N}\left(\mathbf{z}_k; h\left(\mathbf{x}_k^{(a)}\right), \mathbf{R}\right) \mathcal{N}\left(\mathbf{x}_k^{(\mathbf{a})}; \mathbf{x}_{k|k-1}^{(\mathbf{a})}, \mathbf{P}_{k|k-1}^{(\mathbf{a})}\right) \mathrm{d}\mathbf{x}_k^{(a)}} \mathrm{d}\mathbf{a} \\
&\approx \int \frac{\mathcal{N}\left(\mathbf{z}_k; \mathbf{H}\mathbf{x}_k^{(a)}, \mathbf{R}\right) \mathcal{N}\left(\mathbf{x}_k^{(\mathbf{a})}; \mathbf{x}_{k|k-1}^{(\mathbf{a})}, \mathbf{P}_{k|k-1}^{(\mathbf{a})}\right)}{\int \mathcal{N}\left(\mathbf{z}_k; \mathbf{H}\mathbf{x}_k^{(a)}, \mathbf{R}\right) \mathcal{N}\left(\mathbf{x}_k^{(\mathbf{a})}; \mathbf{x}_{k|k-1}^{(\mathbf{a})}, \mathbf{P}_{k|k-1}^{(\mathbf{a})}\right) \mathrm{d}\mathbf{x}_k^{(a)}} \mathrm{d}\mathbf{a} \\
&= \int \frac{\mathcal{N}\left(\mathbf{z}_k; \mathbf{H}\mathbf{x}_{k|k-1}^{(a)}, \mathbf{S}\right) \mathcal{N}\left(\mathbf{x}_k^{(\mathbf{a})}; \mathbf{x}_{k|k-1} + \mathbf{W}\left(\mathbf{z}_k - \mathbf{H}\mathbf{x}_{k|k-1}^{(a)}\right), \mathbf{P}_{k|k-1}^{(\mathbf{a})} - \mathbf{WSW}\right)}{\int \mathcal{N}\left(\mathbf{z}_k; \mathbf{H}\mathbf{x}_{k|k-1}^{(a)}, \mathbf{S}\right) \mathcal{N}\left(\mathbf{x}_k^{(\mathbf{a})}; \mathbf{x}_{k|k-1} + \mathbf{W}\left(\mathbf{z}_k - \mathbf{H}\mathbf{x}_{k|k-1}^{(a)}\right), \mathbf{P}_{k|k-1}^{(\mathbf{a})} - \mathbf{WSW}\right) \mathrm{d}\mathbf{x}_k^{(a)}} \mathrm{d}\mathbf{a} \\
&= \int \mathcal{N}\left(\mathbf{x}_k^{(a)}; \mathbf{x}_{k|k-1} + \mathbf{W}\left(\mathbf{z}_k; \mathbf{H}\mathbf{x}_{k|k-1}^{(\mathbf{a})}\right), \mathbf{P}_{k|k-1}^{(\mathbf{a})} - \mathbf{WSW}\right) \mathrm{d}\mathbf{a}
\end{aligned}
\tag{19}
$$

Line 2 of (19) yields due to the Bayes rule. In line 3 we define the extended state vectors by $\mathbf{x}_k^{(\mathbf{a})} = (\mathbf{x}_k, \mathbf{a})^T$, $\mathbf{x}_{k|k-1}^{(\mathbf{a})} = (\mathbf{x}_{k|k-1}, \bar{\mathbf{a}})^T$ and state covariance $\mathbf{P}_{k|k-1}^{(\mathbf{a})} = \left(\begin{array}{c|c} \mathbf{P}_{k|k-1} & \mathbf{O} \\ \hline \mathbf{O} & \mathbf{C}_a \end{array}\right)$. Linearization of $h(\mathbf{x}_k^{\mathbf{a}}) \approx \mathbf{H}\mathbf{x}_k^{\mathbf{a}} + \mathbf{b} = \mathbf{H}_1\mathbf{x}_k + \mathbf{H}_2\mathbf{a} + \mathbf{b}$ delivers the approximation in line 4. Line 5 follows from the Gaussian refractorization lemma

$$
\begin{aligned}
&\mathcal{N}(\mathbf{z}; \mathbf{H}\mathbf{x}, \mathbf{R}) \mathcal{N}(\mathbf{x}; \mathbf{y}, \mathbf{P}) \\
&\quad = \mathcal{N}(\mathbf{z}; \mathbf{H}\mathbf{y}, \mathbf{S}) \mathcal{N}(\mathbf{x}; \mathbf{y} + \mathbf{W}(\mathbf{z} - \mathbf{H}\mathbf{y}), \mathbf{P} - \mathbf{WSW}),
\end{aligned}
\tag{20}
$$

where $\mathbf{S} = \mathbf{HPH}^T + \mathbf{R}$, $\mathbf{W} = \mathbf{PH}^T\mathbf{S}^{-1}$ with appropriate vectors and matrices $\mathbf{x}, \mathbf{y}, \mathbf{z}$ $\mathbf{H}, \mathbf{P}, \mathbf{R}$.

By extending the target state vector, we can apply the standard EKF or UKF formulas to derive $\mathbf{x}_{k|k}^{(\mathbf{a})}$. Since we are not interested in an update of $\mathbf{a}$ (it is assumed to be independent for different pings), calculation can be simplified for the EKF:

$$\begin{aligned}\mathbf{x}_{k|k} &= \mathbf{x}_{k|k-1} + \mathbf{W}_1(\mathbf{z}_k - h(\mathbf{a}, \mathbf{x}_k)) \\ \mathbf{P}_{k|k} &= \mathbf{P}_{k|k-1} - \mathbf{W}_1\mathbf{S}\mathbf{W}_1^T,\end{aligned} \tag{21}$$

where $\mathbf{S} = \mathbf{H}_1\mathbf{P}_{k|k-1}\mathbf{H}_1^T + \mathbf{H}_2\mathbf{C}_a\mathbf{H}_2^T + \mathbf{R}$, and $\mathbf{W}_1 = \mathbf{P}_{k|k-1}\mathbf{H}_1^T\mathbf{S}^{-1}$. Alternatively, we can use the UKF equivalents of $\mathbf{S}$ and $\mathbf{W}_1$.

Consequences on the Architecture of the MHT. Due to the nonlinearity in the measurement model, approximation techniques are necessary to apply sequential target tracking to multistatic sonar. Comparing the approximation techniques linearization and UT, we find that linearization tends to underestimate the actual errors whilst the UT tends to overestimate, simulation results are presented in Section 8.2.1. Referring to multistatic tracking performance, the two methods based on UT (Cartesian UT and UKF) seem to be preferable and deliver robust tracking results. The analysis with simulated data leads the choice to the UKF as component of the MHT. We prefer the UKF to the Cartesian UT for two reasons.

(1) The UKF method can easily be extended to process additional Doppler information.

(2) Incorporation of the deterministic features (Section 3) is straightforward in the framework of the UKF.

7. Multisensor Fusion

To exploit information from several source/receiver (S/R) pairs an appropriate strategy for *multi*sensor fusion must be developed.

The next two subsections give details of the implementations of the "AND" and "OR" fusion strategy. Then, in a third subsection we develop a new "adaptive" scheme.

7.1. Implementing "AND" Data Fusion in the Framework of MHT. The "AND" fusion strategy fits perfectly in the idea of the MHT. In Figure 6, a cycle of the standard MHT (used in this work) is illustrated. If measurements of k S/R pairs and the same time scan are available we can process the information by sequential updating track hypotheses, this is illustrated in Figure 8(a).

It can be shown that (if measurements of different receivers are uncorrelated) sequentially updating of contact information according to the Kalman filter equation is equal to updating the information together. However, as described in Section 5.2, the MHT is based on suboptimal implementation techniques (each measurement update is followed by hypotheses reduction techniques). Thus, in fact, the order of updating may influence the result.

The "AND" rule does not presume that contact information of every S/R pair is available, rather a track must follow the assumptions about P_D and ρ_F of each single S/R pair.

7.2. Implementing "OR" Data Fusion in the Framework of MHT. The idea to implement the "OR"-rule is to run a single-sensor MHT tracker first at the data sets generated by each S/R pairs. It has to be pointed out that the overall probability of detection for a single bistatic receiver MHT is lower than for the complete multistatic system as described in Section 6.1. Furthermore, the single bistatic receiver MHT cannot exploit triangulation features as described in Section 4.2. The measurements associated with the n-best hypotheses are considered for a second MHT chain that runs on the preprocessed data of all S/R pairs. This second MHT follows the same architecture as described in the above subsection, but the two strategies differ with respect to the calculation of the hypotheses weights and therefore in track evaluation. Here, a hypothesis is not penalized for a missing detection as long as the hypothesis coincides with the detection of at least one S/R pair, see Figure 8(b). The "OR" rule differs from the "AND" rule with respect to the following aspects.

(i) Only measurements associated with an bistatic track are considered in the fusion step.

(ii) A track can be extracted if it follows the assumptions about P_D and ρ_F of a single S/R pair.

7.3. Situational Adaptive Scheme. Both the "OR" and the "AND" fusion strategies are not perfect. Because in the "OR" fusion strategy the MHTs do not have a direct access to all multistatic contact data, the "OR" results do not fully exploit the multistatic measurement setup. The "AND" fusion is very sensitive with respect to an inadequate measurement modelling that could result in an inadequate description of the measurement error or a bias (see also Section 4.2). Especially, "AND" fusion is sensitive with respect to the assumption of a fixed P_D. Let us assume a simple scenario, where there are two receivers, but only one receiver delivers contacts of the target. If the assumed P_D is high for both receivers the "AND" fusion strategy will not be able to track the target (since waiting for measurements of the second receiver).

Combining the positive features of both strategies (robustness of the "OR" strategy and precision of the "AND" strategy) leads to an optimal fusion strategy. This requires more precise information about the actual detection of each S/R pair in the multistatic setup (to provide optimal target tracking performance in combination of a low false track rate). Generally such exact knowledge is not available, but indeed some a priori knowledge about the environmental conditions and about the shape of the target exists. We pick up this idea and derive an approach that exploits a priori information for a more realistic description of the P_D (and with this of the likelihood function). Therein the sonar equation provides an interface between a priori knowledge and the target state. The key task with respect to practicability

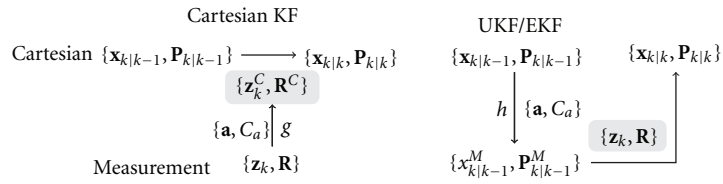

Figure 7: Track update schemes: Cartesian KF (left): Transformation of measurement z_k into Cartesian state; UKF/EKF (right): Transformation of predicted track state into measurement space.

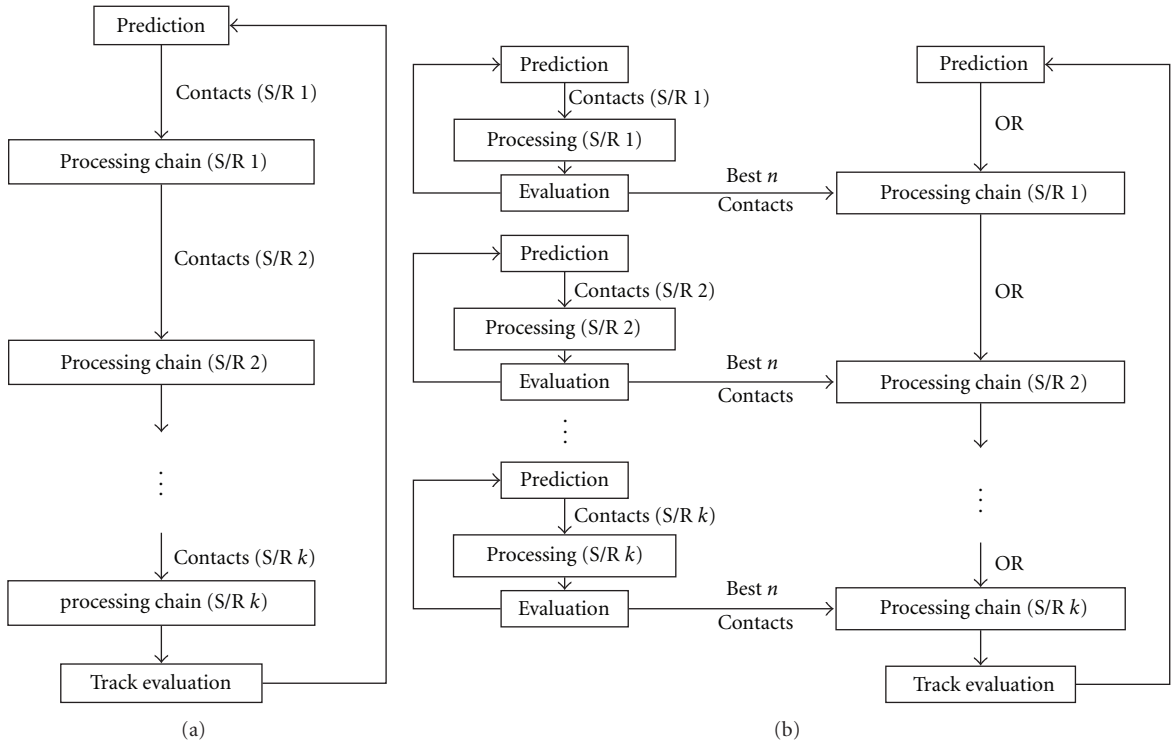

Figure 8: Visualisation of the "AND" (a) and "OR" (b) fusion strategy. A processing chain in the MHT framework contains updating of hypotheses by available contact information and hypotheses reduction techniques.

in the application to sequential target tracking is to estimate correctly the accuracy of the additional information used.

7.3.1. Sonar Equation. The sonar equation combines in logarithmic units (i.e., units of decibels relative to the standard reference of energy flux density of rms pressure of 1 μPa integrated over a period of one second) the following terms:

$$\mathrm{SNR}_{\mathrm{out}} = (\mathrm{S} - \mathrm{TL1} - \mathrm{TL2}) - (\mathrm{NL} - \mathrm{AG}) + \mathrm{TS} \qquad (22)$$

which define signal excess where: S: source energy flux density at a range of 1 m from the source; TL: propagation loss for the range separating the source and the target (TL1) and the target and the receiver (TL2); NL: noise energy flux density at the receiving array; AG: array gain that provides a quantitative measure of the coherence of the signal of interest with respect to the coherence of the noise across the receiving array; TS: target strength whose value strongly depends on the aspect of the target to the source receiver pair, if the target is a long thin cylinder.

For the description of active sonar, the sonar equation has to be applied for the sound path from the source to the target where the received level plus the target strength (TS) is reflected to the receiver. Especially interesting with respect to target tracking are the parts of the sonar equation, which depend on the target position (TL, TS, and NL) and on target position and velocity (TS).

In this paper, we only refer to the sonar equation in the noise limited case, because this is the version used in the algorithms described below. A similar treatment could be proposed for the reverberation limited case.

7.3.2. Implementation of Adaptive Scheme in MHT. The sonar equation describes the functional relationship between the SNR of a measurement and the corresponding target state $\mathbf{x}_k$. In the following, we use the function h_{SNR} with $\mathrm{SNR} = h_{\mathrm{SNR}}(\mathbf{x}_k)$ to express this relationship. We assume the

target-SNR to be Gaussian distributed with a deviation σ_{dB}. This is also assumed to be the deviation of the noise level [14]. Then, the probability of detection is a function of the target state and the detection threshold λ and can be obtained by integration

$$P_{\mathrm{D}}(\mathbf{x}_k, \lambda) = p(h_{\mathrm{SNR}}(\mathbf{x}_k) > \lambda) = \int_{t=\lambda}^{\infty} \mathcal{N}\left(t; h_{\mathrm{SNR}}(\mathbf{x}_k), \sigma_{\mathrm{dB}}^2\right) \mathrm{d}t, \tag{23}$$

assuming Gaussian distribution. Because P_{D} depends on the target's location and aspect, which is exactly what a target tracking algorithm provides as prediction, we use the tracking knowledge when calculating the P_{D} value. Therefore, let $\mathbf{B}_k$ denote the interpretation of the track history up to time t_k; that is, $\mathbf{B}_k$ consists of the events e_i^s, $s = 1, \ldots, k$:

$$e_i^s = \begin{cases} \text{measurement } z_s^i \text{ belongs to target} & \text{if } i \neq 0 \\ \text{target was not detected at time } s & \text{if } i = 0. \end{cases} \tag{24}$$

For each hypothesis branch of the MHT, we compute the expected probability of target detection e_k at time t_k given its respective measurement history $\mathbf{B}_{k-1}$ and the hypothesis of target existence $\mathcal{H}_1$. Thus, the weighting of a hypothesis branch is influenced by the modelling of the detection performance

$$\begin{aligned} p(e_k \mid \mathbf{B}_{k-1}, \mathcal{H}_1) &= \int p(e_k, \mathbf{x}_k \mid \mathbf{B}_{k-1}, \mathcal{H}_1) \mathrm{d}\mathbf{x}_k \\ &= \int p(e_k \mid \mathbf{x}_k, \mathbf{B}_{k-1}, \mathcal{H}_1) p(\mathbf{x}_k \mid \mathbf{B}_{k-1}, \mathcal{H}_1) \mathrm{d}\mathbf{x}_k \\ &= \int \int_{t=\lambda}^{\infty} \mathcal{N}\left(t, h_{\mathrm{SNR}}(\mathbf{x}_k), \sigma_{\mathrm{dB}}^2\right) \mathrm{d}t \mathcal{N}\left(\mathbf{x}_k; \hat{\mathbf{x}}_{k|k-1}, \hat{\mathbf{P}}_{k|k-1}\right) \mathrm{d}\mathbf{x}_k \\ &\approx \int \int_{t=\lambda}^{\infty} \mathcal{N}\left(t - b, H\mathbf{x}_k, \sigma_{\mathrm{dB}}^2\right) \mathrm{d}t \mathcal{N}\left(\mathbf{x}_k; \hat{\mathbf{x}}_{k|k-1}, \hat{\mathbf{P}}_{k|k-1}\right) \mathrm{d}\mathbf{x}_k \\ &= \int_{t=\lambda}^{\infty} \mathcal{N}\left(t - b, H\hat{\mathbf{x}}_{k|k-1}, \sigma_{\mathrm{dB}}^2 + H\hat{\mathbf{P}}_{k|k-1}H^T\right) \mathrm{d}t, \end{aligned} \tag{25}$$

where $\hat{\mathbf{x}}_{k|k-1}$ and $\hat{\mathbf{P}}_{k|k-1}$ denote the estimated target state and covariance respective to the interpretation history $\mathbf{B}_{k-1}$. Row 4 results from row 3 by linearization of h_{SNR} by $h_{\mathrm{SNR}}(\mathbf{x}_k) \approx b + \mathbf{H}\mathbf{x}_k$. The last equality holds due to the Gaussian refactorization lemma (20). The first term at row 4 becomes independent of the target state $\mathbf{x}_k$ whilst the second term is a probability density of $\mathbf{x}_k$, thus the integral is 1.

The pdf is a function of the predicted target state and of the accuracy in this estimate. Thus, the considered Gaussian density becomes flatter with decreasing knowledge about the target state. In the limiting case, the probability is .5.

Usually, the functional relationship in h_{SNR} cannot be described by a simple function. Noise measurements in each bearing and for each receiver and the output of target strength and propagation loss modelling software are used to calculate the actual value of $h_{\mathrm{SNR}}(\mathbf{x}_k)$. Since the derivation, presented above, utilizes the linearization of h_{SNR}, we would need to calculate the derivatives of h_{SNR} with respect to the target state components. However, h_{SNR} is generally a strongly nonlinear function, thus the linearization may be problematic. Replacing the linearization by UT to derive $\mathbf{H}\hat{\mathbf{P}}_{k|k-1}\mathbf{H}^T$ makes it possible to apply the approach without looking deeper into the function h_{SNR}; thus, we can even process tabular entries.

7.4. Fusion of FM and CW Contacts. During the experiments with the deployable multistatic sonar systems, FM and CW signals were transmitted simultaneously. In this case, when regarding to the same target, source and receiver geometry, the values for TL, TS, and NL are quite comparable for both signals. Thus, fusion of FM and CW contacts according to the "AND" rule seems to be straightforward. We can exploit these geometrical similarities but need to consider some differences resulting from the types of signals. Whilst with FM a good range resolution is obtained, the CW delivers additional Doppler information, but with lower range resolution. As a consequence of the poor resolution in range, we decided that CW contacts will not be used for track initialisation. Furthermore, the probability of detection (P_{D}) of a CW measurement is not only dependent on the SNR of the target (Section 7.3), but is additionally dependent on the measured Doppler value [2]. If the Doppler of the target is close to the Doppler of the background, the target is in the so-called clutter notch and the probability of detection is low. The eventuality that a target is in the Clutter notch does not only concern nonmoving targets, but may also appear due to geometrical reasons. In particular, in bistatic applications, these geometrical clutter notches take shape [15] and make demands on regarding to the phenomena of the clutter notch. Let $\dot{r}_{\mathrm{T}}$ be the range rate of the target and $\dot{r}_{\mathrm{C}}$ the range rate of the corresponding background. Using the modelling assumption in [2], we express the P_{D} depending on the distance $n_{\mathrm{C}}(\mathbf{x}_k) = |\dot{r}_{\mathrm{T}} - \dot{r}_{\mathrm{C}}|$, on a characteristic sensor information, the minimum detectable velocity (MDV), and a part $p_{\mathrm{D}}(\mathbf{x}_k)$, that can either be chosen to be fixed or SNR adaptive (see [2] for details)

$$\begin{aligned} P_{\mathrm{D}}(\mathbf{x}_k) &= p_{\mathrm{D}}\left[1 - \exp\left(-\ln(2)\left(\frac{|\dot{r}_{\mathrm{T}} - \dot{r}_{\mathrm{C}}|}{\mathrm{MDV}}\right)^2\right)\right] \\ &= p_{\mathrm{D}}\left(1 - \frac{\mathrm{MDV}}{\sqrt{\ln(2)/\pi}} \mathcal{N}\left(0; n_{\mathrm{C}}(\mathbf{x}_k), \frac{\mathrm{MDV}^2}{2\ln(2)}\right)\right). \end{aligned} \tag{26}$$

In analogy to (25), we can calculate the probability of target detection, as is needed for the likelihood function

$$
\begin{aligned}
p(e_k \mid \mathbf{B}_k, \mathcal{H}_1) &= \int p(e_k, \mathbf{x}_k \mid \mathbf{B}_{k-1}, \mathcal{H}_1)\mathrm{d}\mathbf{x}_k \\
&= \int p(e_k \mid \mathbf{x}_k, \mathbf{B}_{k-1}, \mathcal{H}_1)p(\mathbf{x}_k \mid \mathbf{B}_{k-1}, \mathcal{H}_1)\mathrm{d}\mathbf{x}_k \\
&= \int p_{\mathrm{D}}\left(1 - \frac{\mathrm{MDV}}{\sqrt{\ln(2)/\pi}}\mathcal{N}\left(0; n_{\mathrm{C}}(\mathbf{x}_k), \frac{\mathrm{MDV}^2}{2\ln(2)}\right)\right)\mathcal{N}\left(\mathbf{x}_k; \hat{\mathbf{x}}_{k|k-1}, \hat{\mathbf{P}}_{k,k-1}\right)\mathrm{d}\mathbf{x}_k \\
&\approx p_{\mathrm{D}}\left(1 - \frac{\mathrm{MDV}}{\sqrt{\ln(2)/\pi}}\mathcal{N}\left(-b; N_{\mathrm{C}}\hat{\mathbf{x}}_{k|k-1}, \frac{\mathrm{MDV}^2}{2\ln(2)} + N_{\mathrm{C}}\hat{\mathbf{P}}_{k|k-1}N_{\mathrm{C}}^T\right)\right).
\end{aligned}
\tag{27}
$$

From row three to four, we exploit the Gaussian refactorization lemma and a approximation by linearization of $n_{\mathrm{C}}(\mathbf{x}_k) = b + N_{\mathrm{C}}\mathbf{x}_k$. The derivation shows that only the predicted state estimate and state covariance influences the considered probability of detection.

For the fusion step the CW contacts are similarly processed to FM contacts. But the modelling assumption of the P_{D} (26) will have influence on hypothesis weighting and even on the track update process. The update formulas are derived according to the Bayes formalism in [2]. As it can be seen in (26) the fictitious "measurement" that the target is in the clutter notch, is Gaussian distributed due to the modelling assumptions and can therefore be processed as an additional "measurement" information. The EKF approximation (utilized in [2]) is again replaced by an UKF approach, see [15]. The fusion of CW and FM contacts is an example for a situational adaptive fusion scheme as motivated in Section 7.3. A priori knowledge about the clutter notch is imbedded in the tracking algorithm. But, the fusion of FM and CW goes even one step further by defining the fictitious "measurement". For the situational adaptive scheme presented in Section 7.3, only hypothesis weighting but not state estimation is influenced.

The "AND", "OR", and situational adaptive fusion of measurements of different S/R pairs can easily be adapted to account for additional CW contacts.

For the "AND" fusion strategy, the consideration of CW contacts is straightforward; all available contact files (FM and CW contacts) are exploited for sequentially updating the hypothesis tree (regarding to the characteristics of the CW signal); we later refer to this as "AND" fusion strategy of FM and CW contacts.

Similarly, the "situational adaptive fusion of FM and CW contacts" is straightforward. The fixed P_{D} settings for the FM and the fixed part of the P_{D} for the CW will be estimated from the sonar equation.

The "OR" fusion strategy is adapted to combine FM and CW contacts in the following way (later to be referred to as "OR" fusion strategy of FM and CW contacts):

(i) tracking of FM and CW contacts of each S/R pairs ("AND" fusion of FM and CW contacts);

(ii) taking the FM contacts associated to tracks and running a second instance of the MHT.

Interesting with respect to the phenomena of the clutter notch in multistatic sonar are nonmoving targets such as a wreck. Wrecks produce continuous FM contacts, whilst they are not detected by the CW signal. This is different in typical scenarios of ground moving target tracking and allows a look at the phenomena of the Clutter notch from a different point of view. We will discuss results in Section 8.1.4.

8. Data Analysis

In the previous sections, many adaptations of the MHT structure have been developed. In this section, we demonstrate the necessity for making these amendments. There are several data sets from measurements at sea available. We apply them to the derived algorithms, stepwise increasing the level of precision of the sensor modelling. We show that the tracking performance increases when correctly modelled details of the sensor model are added. In its final state, the algorithm is able to deliver high precision target state information and a very low false alarm rate. However, measurement at sea is cost and time intensive. Not all statistical aspects of the algorithm's design can be significantly answered by the limited data set. Therefore, we augment the experimental data by numerical simulations in order to evaluate the different possibilities for necessary numerical approximations inside the tracking process. We will also see an example for the necessity to improve the motion model: since our motion model does not include possible turns and since inside the tracking algorithm only small uncertainties due to precise modelling exists, strong manoeuvres of the target seem to decrease the quality of the performance of the tracker with the better sensor model, see Section 8.1.4(a). We propose to rather improve the motion model, see for example [16], instead of arguing for a more robust, but imprecise sensor model.

8.1. Data Analysis with Experimental Multistatic Sonar Data. In this section, we test the different adaptations of the MHT algorithm. Table 2 provides an overview of the different modes and specifies the section of more detailed information.

Following the ordering in the tabular, we will refer to different versions of the MHT in the following by: (1) TiCor, (2) DoCor (The abbreviation DoTiCor is used,

Table 2: Overview of different versions of the multistatic MHT.

Deterministic features		Multisensor Fusion			Fusion of CW and FM		
Timing	Range-Doppler Ambiguity	P_D fixed "AND"	P_D fixed "OR"	P_D adaptive	P_D fixed "AND"	P_D fixed "OR"	P_D adaptive
Section 3.1	Section 3.2	Section 7.1	Section 7.2	Section 7.3	Section 7.4	Section 7.4	Section 7.4

when correction for timing and Range/Doppler ambiguity is applied simultaneously), (3) "AND" fusion of FM, (4) "OR" fusion of FM, (5) adaptive fusion of FM, (6) "AND" fusion of FM and CW, (7) "OR" fusion of FM and CW, and (8) adaptive fusion of FM and CW. The measurement update step is always realised by the UKF as motivated in Section 6.2. Unless specified otherwise the different fusion strategies are applied in combination with the DoTiCor approach.

8.1.1. Description of the Data Sets. In the course of NURC's project on deployable multistatic active sonar, two major sea trials were conducted: PreDEMUS'06 and SEABAR 07. Measurements at sea have been executed within the Scientific Program of Work at the NATO Undersea Research Centre (NURC). Since the data have been distributed among several research institutions in NATO, we use the original names given to the data sets for potential further reference.

Note. Experiments at sea generate only a limited set of data and are conducted under specific equipment and safety constraints. For further sensitivity studies and specific statistical performance analysis we added simulated data sets; Section 8.2.

Common to all data sets is the usage of the deployable buoy system (Figure 1, called DEMUS).

(i) *DEMUS Receivers.* The systems are built on a frame of 9 arms; each arm is made up of 7 acoustic outputs or staves. Each of these acoustic outputs is produced by summing three vertical hydrophones. The lateral spacing of hydrophones is variable and can be set remotely. The system is designed to operate in the range 2–5 kHz. The level of the "Input Referred Noise" across the band of interest is lower than the noise level at calm seas, making the receiver a high-quality measurement system. The system is bottom tethered, typically at 100 m depth. Nonacoustic output of the system contains of depth, compass, and tilt.

(ii) *DEMUS Transmitter.* The transmitter is tethered in the same way as the receiver. The operating frequency range is 2–4.2 kHz. It is constructed from 8 FFRs, where weightings can be applied to outputs for vertical steering and beam shaping. The typical battery life is 500 ping seconds.

Also, common to all data sets is that an artificial target was used, called echo-repeater (or E/R). The E/R was towed by a surface vessel at a depth of 80 m. It retransmits received source signals with a specified amplification (TS_{ER}) and a certain delay. For the delay, the contact data have been already corrected. Details of this correction process are omitted here, but it is obvious that a high TS_{ER} level is needed to identify uniquely the corresponding contacts. Resulting received signal-to-noise ratios (SNR) are unrealistically high, but can be decreased by simply inserting lower values in the corresponding data structure of a contact [17]. However, with this procedure it is possible to generate contacts for the target that in a real scenario would not occur because their SNR would correspond to a threshold setting for contact generation that is too low.

For data analysis, we consider five data sets based on PreDEMUS'06 B01, SEABAR 07 A01, and A56:

(a) *PreDEMUS'06 B01.* The setup of PreDEMSUS'06 is shown in Figure 9(a), a single source and three receivers were installed. E/R signals are detected within a moderate noise background generated by distant shipping. DT and IT are set to 10 dB for FM contacts. CW contacts are all taken without a threshold. The corresponding input files for each source receiver pair contain about 60 contacts per ping for FM and about 90 contacts per ping for CW.

(b) *SEABAR 07 A01_50.* The setup is shown in Figure 9(b), detections of two receivers and one source are given. E/R signals are detected within a high reverberation level plus time-varying directional high noise levels from close shipping. The data set contains the best 50 contacts of the FM processing and all (about 100) contacts from the CW processing. IT is set to 10 dB.

(c) *SEABAR 07 A01_TS.* As in SEABAR 07 A01_50 and A01_10dB, but now the SNR values of the target contacts have been reduced [17]. The tracker has to process about 500 contacts per ping and each S/R pair for the FM and again about 100 contacts for the CW. A threshold of 2 dB is set to the reduced E/R contacts causing a reasonable number of missed detections. The IT was again 10 dB.

(d) *SEABAR 07 A56_50.* The setup is shown in Figure 9(c), detections of two receivers and one source are given. During Run A56, the measurement was made in bad weather conditions. We use the time synchronized data set, but with the original target SNRs [17]. It contains the best 50 contacts of the FM processing and all contacts from the CW processing (about 100). IT is set to 10 dB.

(e) *SEABAR 07 A56_all.* Same as SEABAR 07 A56_50, but the data set contains all FM contacts (about 500) and all CW contacts. IT is set to 10 dB.

8.1.2. Performance Metrics. In the following, we will assess the performance of the proposed extensions by applying the different modes of the algorithms to these data sets. Changes in performance should be made visible when calculating measures like *track duration*, *track fragmentation*, *latency*, *false track rate,* and *estimation performance*. We will correspond to track duration, latency, and track fragmentation by indicating the time of track extraction (TE) and termination (TT). Thus, the track latency corresponds to the TE time; the track duration can be calculated by (TT-TE), and track fragmentation is demonstrated by indication of several times of TT and TE. This is different from the track duration metric defined in [18], which counts for the measurement associations since initialization of a tentative track.

The total track rate (mean number of tracks per ping) that is utilized in this paper counts for all extracted tracks (including the true target track), it is directly related to the false track rate.

Estimation performance is either specified by calculating the estimation errors or illustrated by direct comparison of target and track trajectory.

8.1.3. Results for PreDEMUS'06 B01. The data set B01 was analysed by detailed postprocessing to determine the exact position of the E/R sound source, thus quite accurate truth information is available.

(a) *Impact of Deterministic Features—SEABAR 07 A01_50 and SEABAR 07 A01_10 dB.* The algorithms DoCor, TiCor, and DoTiCor, as defined in Section 3 are applied and their performance is compared to the versions without correction (NoCor). All results correspond to fusion of FM contacts of RX1, RX2 and RX3 according to the "AND" fusion strategy (CW measurements are not considered). In Figure 10(a), the estimation error of the algorithms is plotted, demonstrating that the corrections are necessary. Figure 10(b) demonstrates this by plotting the results of the DoTiCor and NoCor approach in the 2D plane. Results for the correction of the Doppler ambiguity are shifted. The bias in the range measurement due to the frequency shift is compensated.

Remark. The effect of the corrections depends on the given geometry.

(b) *Results of Different Fusion Strategies—PreDEMUS'06 B01.* Within the noise background and the chosen false alarm rate, detections from receiver RX1 and RX3 are not possible due to the large distance to the target for the first 50 pings, see Figure 11. Clearly, the "AND" strategy suffers from missing detections in at least a second receiver. Close to ping 30, detection was missed for all three receivers for about 10–20 pings. After that the target is quite frequently detected by all three receivers.

Following the description of the fusion strategies in Section 7 we apply the different fusion approaches to the data set of PreDEMUS'06 B01 (all utilizing the DoTiCor approach). Results are shown in Table 3.

The missed detections of RX1 and RX3 in the beginning affect the tracking results. Thus, when pursuing the "AND" fusion strategy (1st row), the target track is not extracted in an initial phase of about 50 pings. As expected, the "OR" fusion strategy (2nd row) gives better results in this region, since contact information of RX2 is sufficient for track extraction.

For the situational adaptive scheme (3rd row), the values for TL were calculated according to the distance between source, receiver, and estimated target state. The NL level was fixed (assuming a stationary noise background) and since an E/R does not have aspect-dependent target strength, the TS value was also kept constant. In the considered scenario the situational adaptive scheme proves to be an adequate compromise between "AND" and "OR" fusion strategy, it provides good track duration and low false track rate. For both approaches, "OR" fusion and situational adaptive, track fragmentation occurs at ping 28; this is when all three S/R pairs miss detections.

The combination of FM and CW contacts (4th row) results in a significant reduction of false tracks. Additionally, comparison of only FM (1st row) and FM and CW (4th row) shows improvements with respect to track latency, when processing the CW contacts.

Estimation performance was quite comparable for all approaches.

8.1.4. Results for SEABAR A01_50. For the data from A01 only positional information about the E/R towing vessel were available. Thus the E/R (the target) is located behind the position of the vessel depended on the length of the cable. To prevent incorrect estimation of the E/R position we compare our results with the position of the towing vessel.

(a) *Impact of Deterministic Features—SEABAR 07 A01_50.* Comparing the results of the DoTiCor approach and the uncorrected version of the MHT (NoCor), we observe an offset in Cartesian estimates, as also noted for PreDEMUS'06 B01. Unfortunately, improvements in localization error can not be verified due to inaccuracies of the truth information. This has be discussed in more detail in [19], it was shown that the application of the DoTiCor approach additional causes degrading tracking performance (from which the MHT can recover) during the first target manoeuvre. The approach seems to be less robust against deviations from the motion model. This is a consequence of the influence that the estimated Doppler has on the range measurement.

(b) *Results of Fusion Strategies—SEABAR A01_50.* In Figure 12, the target detection performance of RX2 and RX3 is shown. For SEABAR A01_50 (Figure 12(a)), both receivers show overall good detection performance, which was due to the setting of the E/R. RX3 miss the target for the last 10 pings. We start our analysis with tracking FM contacts of each S/R pair only. Results for fusing information of both receivers either according to the "AND" (Figure 13(a)) or "OR" (Figure 13(b)) fusion strategy delivers improved

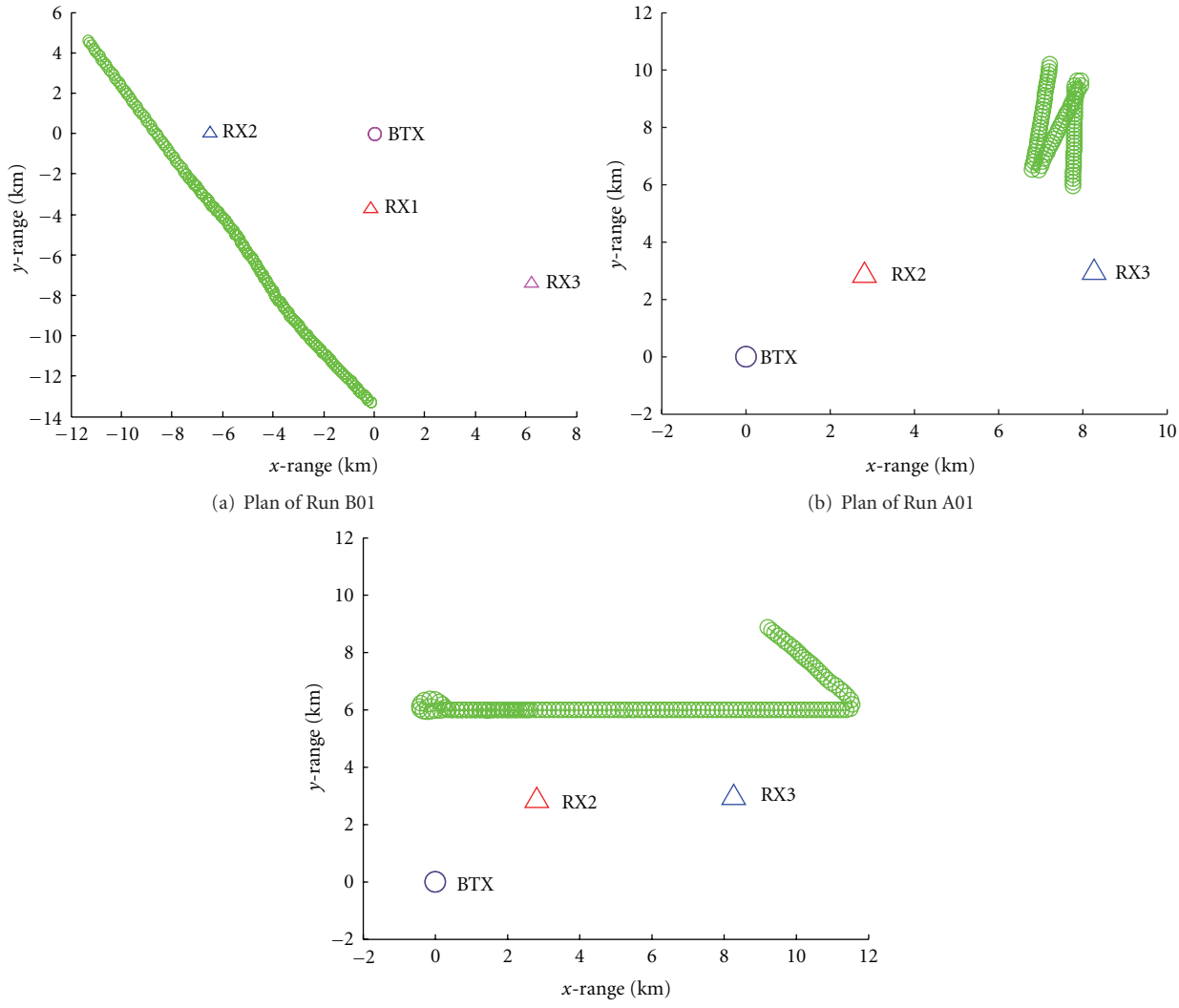

(a) Plan of Run B01

(b) Plan of Run A01

(c) Plan of Run A56

Figure 9: Plan of B01 and the two runs from SEABAR07 transformed in 2D Cartesian; two receivers (RX2 and RX3) and single target (green) and one source (BTX).

Table 3: Tracking results for B01.

Results for B01	Start of track (ping)	End of track (ping)	Mean number of tracks per ping
"AND" fusion of FM (RX1, RX2 and RX3)	53	146	8.16
"OR" fusion of FM (RX1, RX2 and RX3)	23	28	9.17
	46	146	
Situational adaptive fusion of FM (RX1, RX2 and RX3)	20	28	7.06
	48	146	
"AND" fusion of FM and CW (RX1, RX2 and RX3)	50	146	2.54

localisation results compared to the tracking of single S/R pairs. As is observed here, the "AND" fusion rule outperforms the "OR" rule with respect to estimation performance. If considering additional CW contacts, see Section 7.4, we observe improved estimation performance for "OR" fusion (Figure 13(c)). For "AND" fusion (not displayed), estimation performance does not change. However, it still show superior performance.

Table 4 gives summarized details about the tracking performances of the different fusion methods.

For all approaches, we choose the same parameter settings and applied the DoTiCor approach. The "AND" fusion strategy outperforms the "OR" fusion strategy with respect to tracking performance and false track rate. For all approaches we note a significant reduction of the false track rate when considering additional CW contacts.

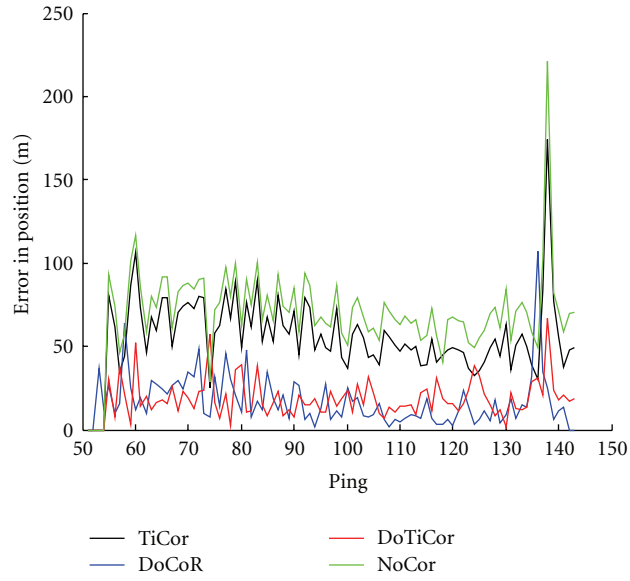

(a) Estimation error for tracking results of B01 using approaches TiCor and DoCor

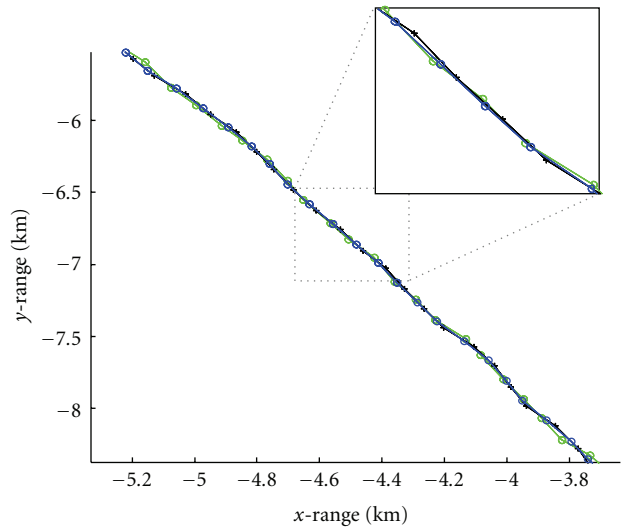

(b) Tracking results of B01 for NoCor and DoTiCor in 2D-Cartesian. The position of the E/R is shown in green

FIGURE 10: Illustration of improvements in estimation performance when accounting for deterministic features. Results correspond to "AND" fusion of FM contacts of RX1, RX2, and RX3. The latency of the target tracks is about 50 pings.

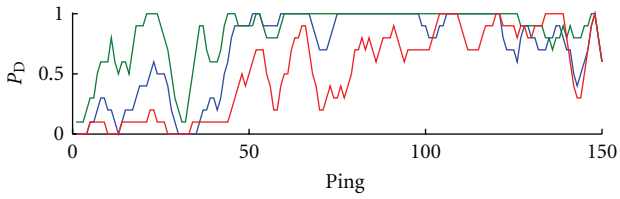

FIGURE 11: Target P_D for RX1 (blue), RX2 (green), and RX3 (red), respectively; The P_D is averaged over 5 pings and over FM and CW. Detection performance of receivers RX1 and RX3 is poor for the first 50 pings due to the large distance to the target.

(c) *Tracking of Bottom Targets—SEABAR 07 A01_50.* In addition to the target contacts, generated by the E/R the data set contains some bottom targets (e.g., wrecks). These targets produce continuous FM echoes and can thus be located precisely. Figure 14(a) shows the 2D tracking output of the "AND" fusion approach of FM and CW contacts of RX2 and RX3. Known target positions are numbered and shown by a blue plus sign. Bottom targets 1, 2, and 6 are found by the MHT. Obviously, the algorithm is able to track fixed targets even when exploiting the CW contacts. Since the Doppler of a bottom target is equal to the Doppler of the background (i.e., zero Doppler for nonmoving sources and receivers), fixed targets will not generate CW contacts. Our algorithm accounts for this effect, since the probability of detection is adaptive to the target movement, see Section 7.4. If no CW contacts are available the hypothesis that the target is nonmoving is strengthened. Furthermore, hypotheses with high velocities are penalized. Figures 14(b) and 14(c) show results for the Clutter targets 1 and 2. The red and the blue dots represent contact information of the receivers RX2 and RX3 that are transformed into Cartesian coordinates. Due to the proximity to the target, contacts formed by RX2 are especially suited for localising target 1, see Figure 14(b). Contacts of RX3 show a larger diffusion. Thus, we cannot see much advantage from the fusion of contacts of the both receivers. The achieved localisation accuracy can be traced back to the measurements of RX2. Another effect can be studied on the basis of the bottom target 2, Figure 14(c). This target shows a convenient geometry to exploit the fusion of contacts of the two receivers. Contact information of a single receiver diffuses at a line (according to the angular uncertainty) whereas the tracking result lies in the intersection of those two lines and is therefore very accurate.

8.1.5. Results for SEABAR 07 A01_TS. For the data set SEABAR 07 A01_TS the SNRs of the target contacts are about 10 dB lower than the original ones, whilst the SNR of the non-target contacts was retained. To preserve a reasonable detection probability of our target, we need to consider a larger amount of contacts in the tracking algorithm. The detection performance is illustrated in Figure 12(b). Both receivers show overall good detection performance, beside of some missed detections of RX3 near to ping 40. We apply the "AND" fusion strategy of FM and CW contacts of RX2 and RX3 to this data set, since it has shown the best performance in application to SEABAR A01_50. The increasing false alarm rate has an effect on track extraction and track maintenance (compare Section 5) and leads to a track loss in our application: Here, the reason for the track loss is an increased noise level at RX2

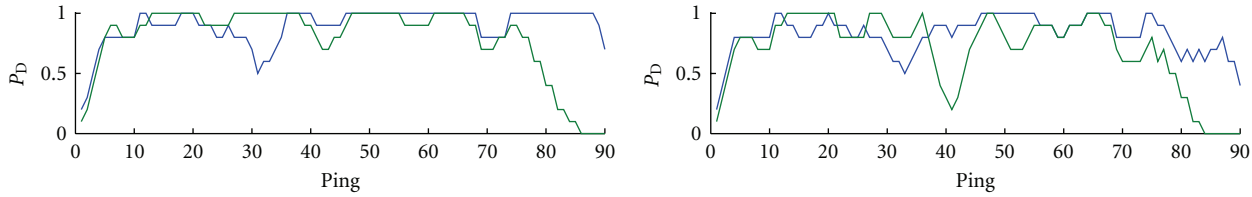

(a) SEABAR A01_50 (b) SEABAR A01_TS

Figure 12: Target P_D for RX2(blue) and RX3(green). (a) shows the detections performance for the original SNRs of target contacts in the data set SEABAR A01_50, in (b) the SNRs are about 10 dB reduced (SEABAR A01_TS). The P_D was averaged over 5 pings and over FM and CW.

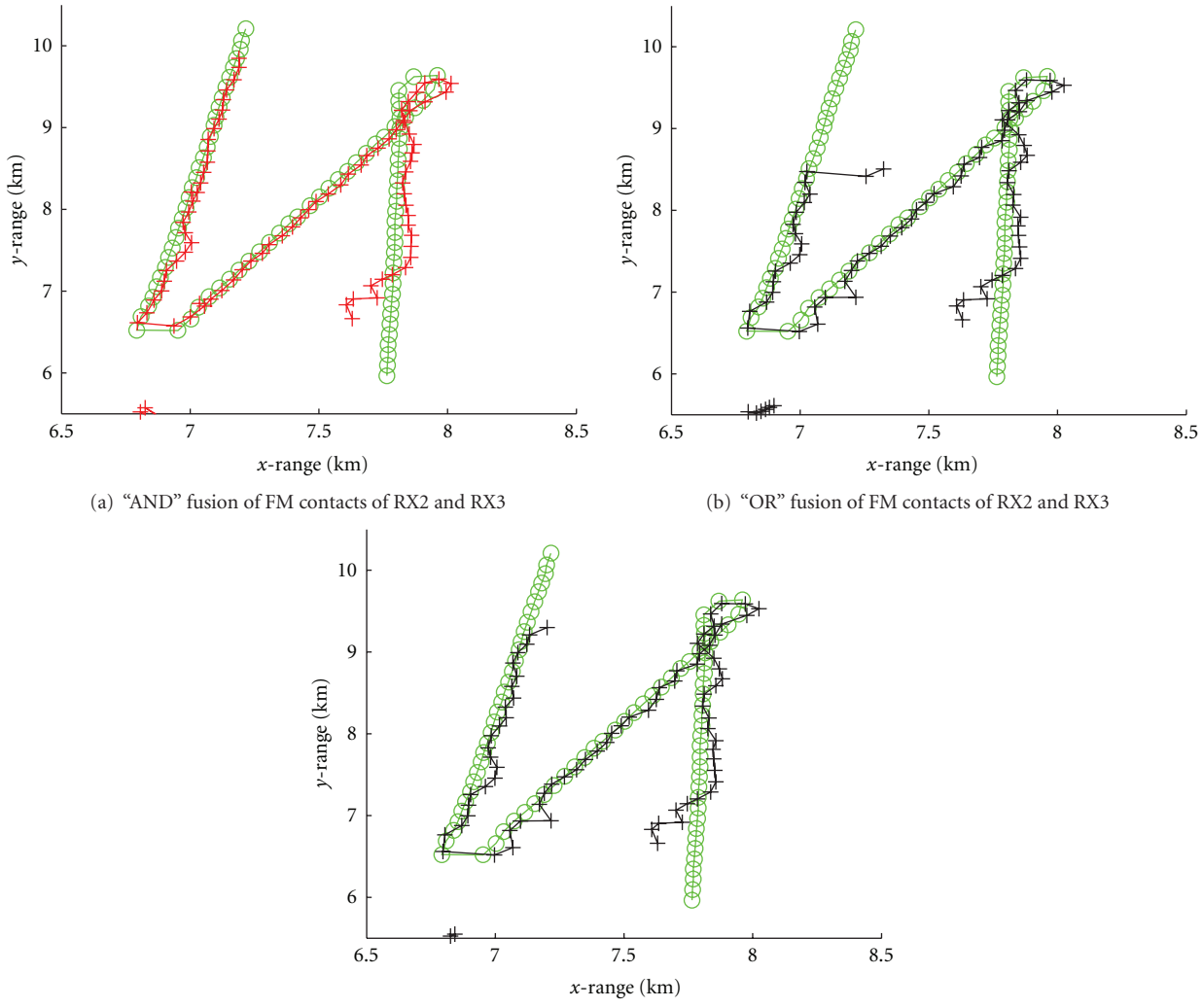

(a) "AND" fusion of FM contacts of RX2 and RX3

(b) "OR" fusion of FM contacts of RX2 and RX3

(c) "OR" fusion of FM and CW contacts of RX2 and RX3

Figure 13: Tracking results using only FM contacts (a)-(b) and FM and CW contacts (c); target area is shown in detail; tracks are illustrated by plus signs versus the position of the towing ship (green circles).

that occurs temporarily (after the first target manoeuvre) due to a passing merchant vessel. Exploiting this additional environmental information inside the tracking algorithm leads to improved (i.e., continuous) tracking performance. In order to apply the situational adaptive approach, the SNR was estimated by exploiting information about the noise level and the transmission loss. The TS value was kept constant.

To make results comparable, the fixed parameter (P_D), which is needed as an input parameter in the "AND" fusion approach, were set to the mean values, chosen by the adaptive scheme. We run the MHT for different assumed values of the

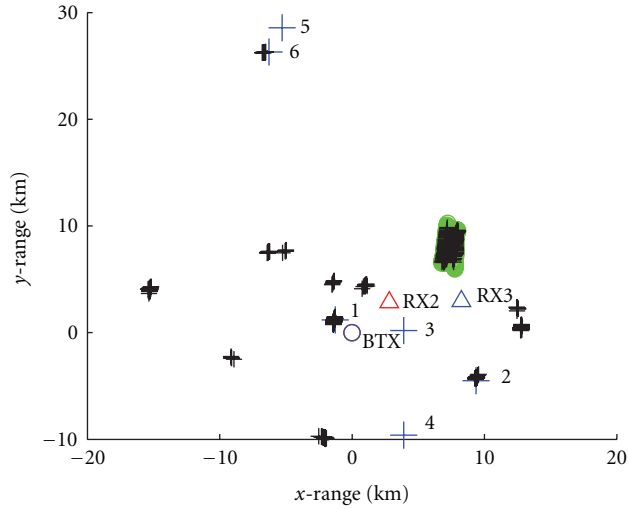

(a) Tracking output (black) of "AND" fusion of FM and CW contacts of RX2 and RX3; the assumed position of the registered fixed targets are shown by a blue plus sign; target 1, 2 and 6 are found by the MHT

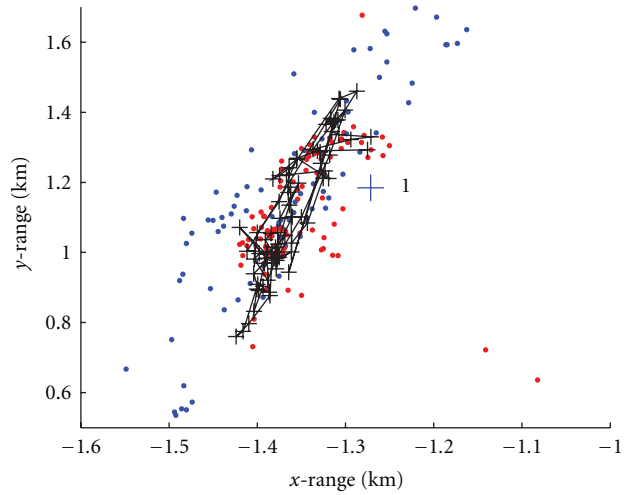

(b) Clutter target 1, FM and CW

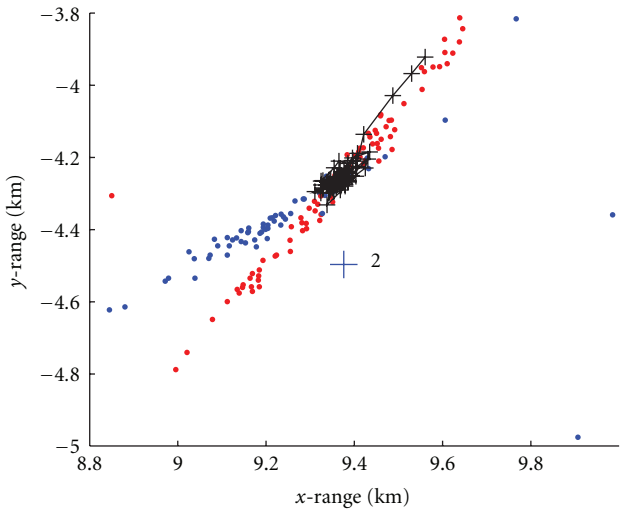

(c) Clutter target 2, FM and CW

Figure 14: Tracking of bottom targets.

Table 4: Tracking results for A01.

Results for A01	Start of track (ping)	End of track (ping)	Mean number of tracks per ping	Figure
FM (RX2)	12	88	10.84	
FM (RX3)	17	80	8.12	
"AND" fusion of FM (RX2 and RX3)	7	88	9.2	Figure 13(a)
"OR" fusion of FM (RX2 and RX3)	16	88	10.7	Figure 13(b)
FM and CW (RX2)	11	88	7.43	
FM and CW (RX3)	7	80	5.28	
"AND" fusion of FM and CW (RX2 and RX3)	6	88	5.15	
"OR" fusion of FM and CW (RX2 and RX3)	11	88	8.3	Figure 13(c)

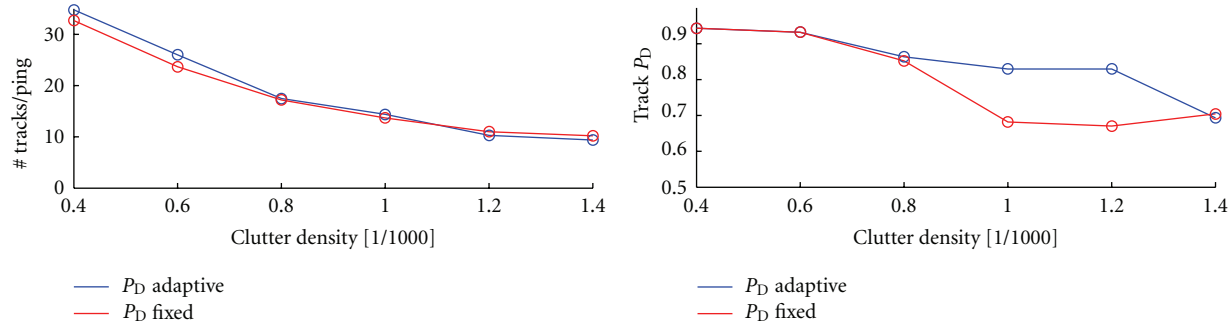

(a) Comparison of false track rate; y-axis shows the mean number of tracks/ping

(b) Comparison of track output P_D

FIGURE 15: Comparison of tracking performance for two different algorithms: "situationally adaptive fusion of FM and CW contacts (P_D adaptive)" and ""AND" fusion of FM and CW contacts (P_D fixed)". Calculations of performance metrics in (a) and (b) are made for the following values of the false alarm density (in #/1000): 0.4, 0.6, 0.8, 1.0, 1.2, 1.4.

false alarm density ρ_F to compare the tracking performance of the two different approaches; the values for the other tracking parameters are identical. In Figure 15, the results are shown. Figure 15(a) shows the mean number of tracks per ping (this is comparable to the false track rate) and Figure 15(b) refers to the track output P_D; that is, percentage of pings for that the target could be tracked. It can be noticed that choosing larger values of ρ_F result in fewer false tracks and worse tracking performance. This is because the algorithm tends to interpret a contact as a false alarm. But whilst for the fixed P_D approach we observe track fragmentation already for small values of the false alarm density (i.e., track was fragmented for $\rho_F > 1/1000$), the P_D adaptive scheme delivers better track quality; we note a higher track output P_D and track-fragmentation occurs for the first time at $\rho_F = 1.4/1000$.

8.1.6. Results for SEABAR A56_50. In similarity to the data of A01, we start with the best 50 contacts for FM as input file of our tracker.

(a) *Impact of Deterministic Features—SEABAR 07 A56_50.* Figures 16(a) and 16(b) displays the tracking performance of the DoTiCor approach (blue circle) and the uncorrected (NoCor) version of the MHT (black plus sign). FM contacts of the two S/R pairs are fused according to the "AND" fusion strategy. As for A01, tracking results are compared to the position of the towing ship (green circle). Again, we note shifted results of the DoTiCor versus the standard approach.

(b) *Results of Fusion Strategies—SEABAR 07 A56_50.* In analogy to SEABAR 07 A01_50, we compare the different fusion approaches (again only for DoTiCor). As for A01, the "AND" fusion strategy (Figures 16(a) and 16(b) only FM) and (Figure 17(b) FM and CW) outperforms the "OR" fusion strategy (Figures 16(c) and 17(a)) in terms of estimation performance. The track is also extracted earlier, but we note some small deviation of track and position of the ship during the first manoeuvre which is caused by an inflexibility due to the movement model, see for example Figure 16(b). A comparison of the false track rates is given in Table 5. For the combination of FM and CW the "AND" rule produces again the least false tracks. For FM only, it produces slightly more. This may be due to the fact that the instationary background produces false contacts for both bistatic setups. Since the "OR" strategy passes through the process of track extraction twice, first for a single S/R pair and second in the fusion step, it is less sensitive to false tracks with a short span of life. Here, it is demonstrated that tracking performance is not only influenced by the fusion strategy, but also by the particular implementation.

TABLE 5: Run A56: comparison of false track rate.

Mean number of tracks per ping	FM	FM & CW
RX2	22.19	14.42
RX3	15.7	9.85
"AND" fusion of RX2 and RX3	24.35	12.09
"OR" fusion of RX2 and RX3	23.36	16.95

8.1.7. Results for SEABAR 07 A56_all. Again, the signal strength of the E/R is very high, such that nearly all target contacts are included in the best 50 contacts. However, considering more measurements in the tracking algorithm (decrease DT) would be more realistic. Results of the "AND" strategy for FM and CW contacts of RX2 and RX3 (approach (7)) are shown in Figure 17(c). As expected, tracking performance is degraded compared to the case of the "best" 50 contacts. This confirms that a large quantity of false alarms influence the parameter settings of the MHT and with this the tracking performance. Also, the false track rate increases to 23.13.

Since track fragmentation does not occur for the run A56, we do not expect improvements by the situational adaptive scheme for this scenario.

8.2. Simulated Data. In this subsection, we try to give more statistics to limited real data sets, but keep important features of real data. Section 8.2.1 addresses the problem arising

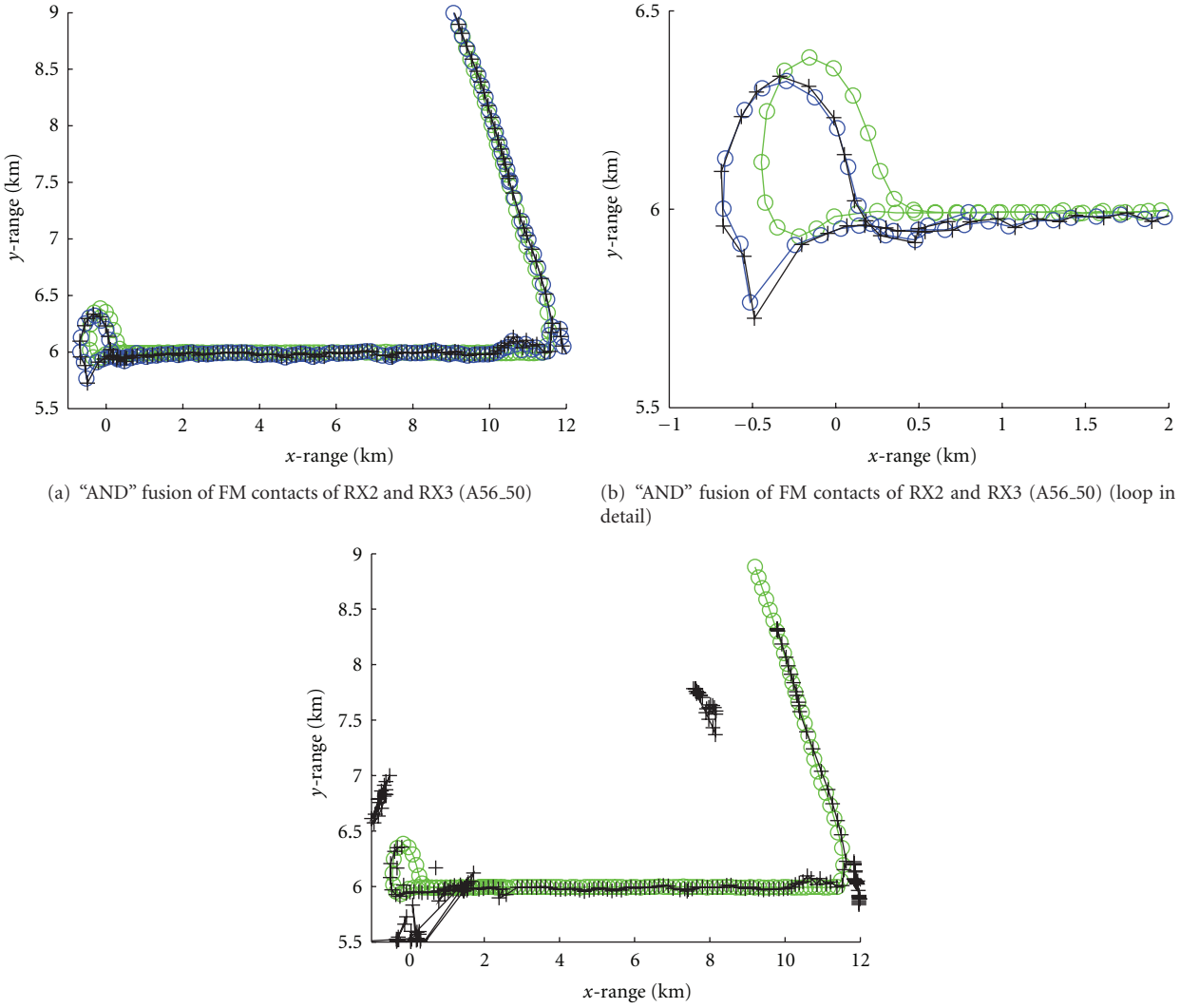

(a) "AND" fusion of FM contacts of RX2 and RX3 (A56_50)

(b) "AND" fusion of FM contacts of RX2 and RX3 (A56_50) (loop in detail)

(c) "OR" fusion of FM contacts of RX2 and RX3 (A56_50)

FIGURE 16: Tracking results for "AND" (a), (b) and "OR" fusion of FM contacts of RX2 and RX3 (c). In (a,b) the approaches NoCor (black plus sign) and DoTiCor (blue circle) are compared. For better visualization false tracks are not displayed: track estimates of the NoCor and DoTiCor approach are shifted. Both approaches show up to be slightly inflexible to derivations from the movement model.

from the nonlinearity of the measurement equation and discusses the different types of KF developed in Section 4. In Section 8.2.2, we test the robustness of the MHT by varying the number of false alarms and in dependency on the measurement accuracy.

8.2.1. Handling the Nonlinearity (Numerical Results). In Section 6.2, we discussed four ways to handle the nonlinear sensor model: the Cartesian approaches based on linearization (Cartesian L) and unscented transform (Cartesian UT), the modified UKF and EKF.

For numerical evaluation, we consider a scenario where the receiver is located at $(-1\,\text{km}, 0\,\text{km})^T$ and the source is at $(1\,\text{km}, 0\,\text{km})^T$. Measurement errors are chosen to be $\sigma_\varphi = 2^\circ$, $\sigma_\vartheta = 2^\circ$, $\sigma_\tau = 0.001$s and $\sigma_{c_S} = 2$ m/s. Additionally, we assume equal and uncorrelated errors for the components of source and receiver position with $\sigma_L = 20$ m; that is, $\mathbf{P}_O = \mathbf{P}_S = \text{diag}(\sigma_L^2, \sigma_L^2)$.

In order to compare the different approaches if implementing the Kalman filter scheme (see Section 6.2), the simulation setup described above is extended in the following way: for each Monte Carlo run a target is inserted at $(2\,\text{km}, 2\,\text{km})^T$. Its constant velocity is sampled from a Gaussian distribution with zero mean and deviation of 5 m/s in $\dot{x}$ and $\dot{y}$ (targets that cross the line between source and receiver are ignored).

The target position estimate discussed in Section 4.1 is used to destine the track initialization point (the UT approximation is used for the UKF and the linearized approximation for the EKF). We initialize target velocities with zero mean and deviation of 5 m/s in each component. In the appendix, we describe how we evaluate the performance of the various algorithmic approaches.

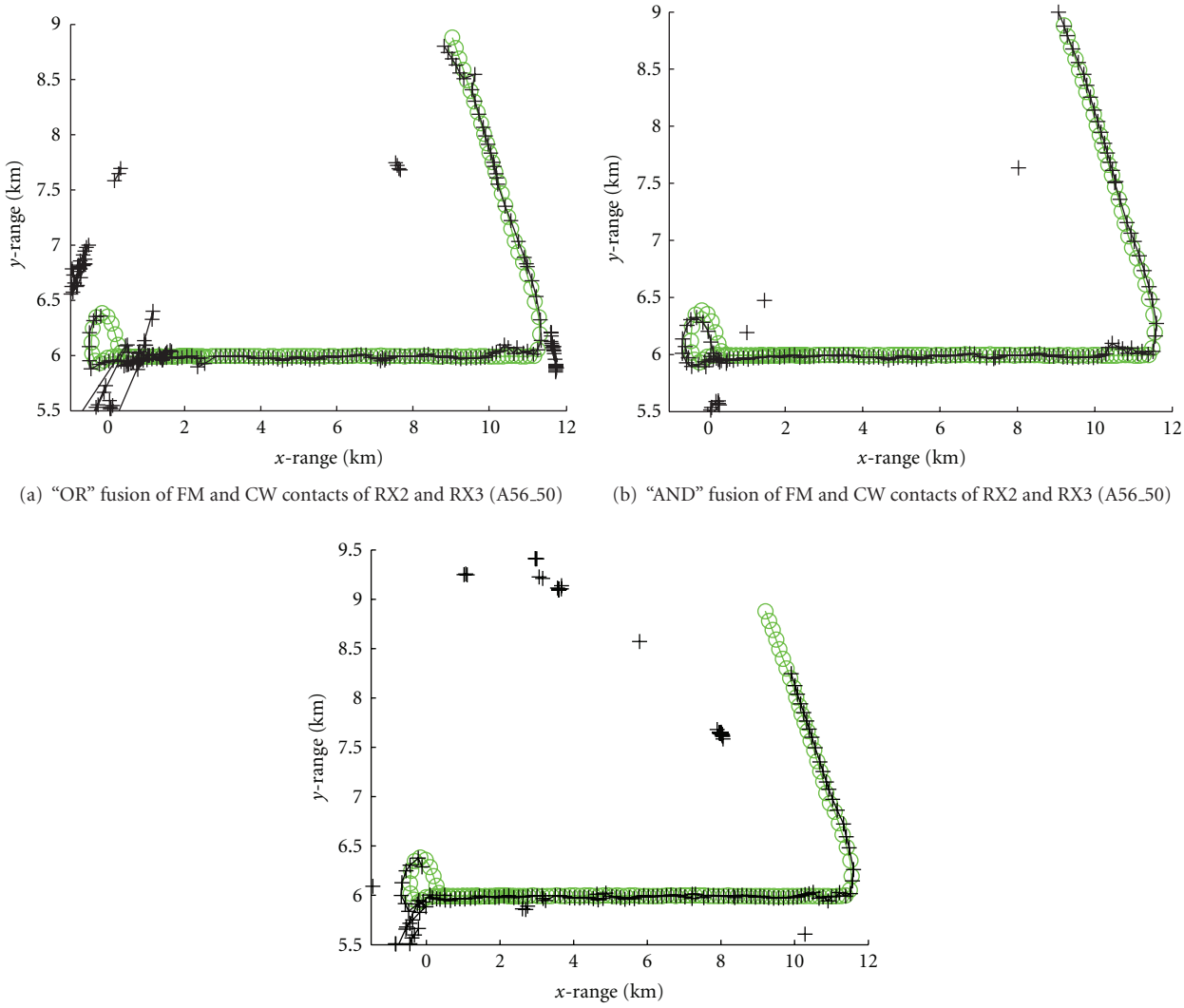

(a) "OR" fusion of FM and CW contacts of RX2 and RX3 (A56_50)

(b) "AND" fusion of FM and CW contacts of RX2 and RX3 (A56_50)

(c) "AND" fusion of FM and CW contacts of RX2 and RX3 (A56_TS)

Figure 17: Tracking results for Run A56_50 and A56_TS (target area in detail).

(a) *Comparing Implementations of the Kalman Filter Scheme.* To analyze the performance of the different types of Kalman filter we run 10^4 Monte Carlo runs. Results of the RMSPOS for the four different tracking approaches are illustrated in Figure 18 and are compared to the CRLB. Figure 18(a) corresponds to the standard settings in the parameter uncertainties and a measurement update rate of 60 seconds, that is time between two consecutive pings is 60 seconds. The two approaches based on the UT show comparable good results. The poor performance of the EKF is remarkable. In Figure 18(b), the influence of the accuracy in source and receiver position ($\sigma_L = 5\,\text{m}$) is considered. When improving the accuracy, we note worse performance of all four approaches. Figure 18(c) corresponds to the same scenario as (b), except for small azimuth and heading errors ($\sigma_\varphi = \sigma_\vartheta = 1^\circ$). Again, we note that the EKF shows worse performance than the other approaches. We also note that, in the initial phase of the tracking scenario, the UKF performance is slightly worse than the performances of Cartesian UT and Cartesian L.

In summary, tracking performance is affected by the measurement and system parameters uncertainty: if the total error is strongly bearing-dependent, that is, large bearing errors or high precision in range, the methods based on UT show superior performance than the methods based on linearization. Additionally, we note that the UKF and the EKF show worse performance than the Cartesian Kalman Filters (Cartesian L and Cartesian UT) during the first pings of the scenario.

These effects are further examined in the next two subsections.

(b) *Dependency on the Measurement and System Uncertainties.* We consider again a single target at position $(2\,\text{km}, 2\,\text{km})^T$. The Cartesian L/UT and EKF/UKF use

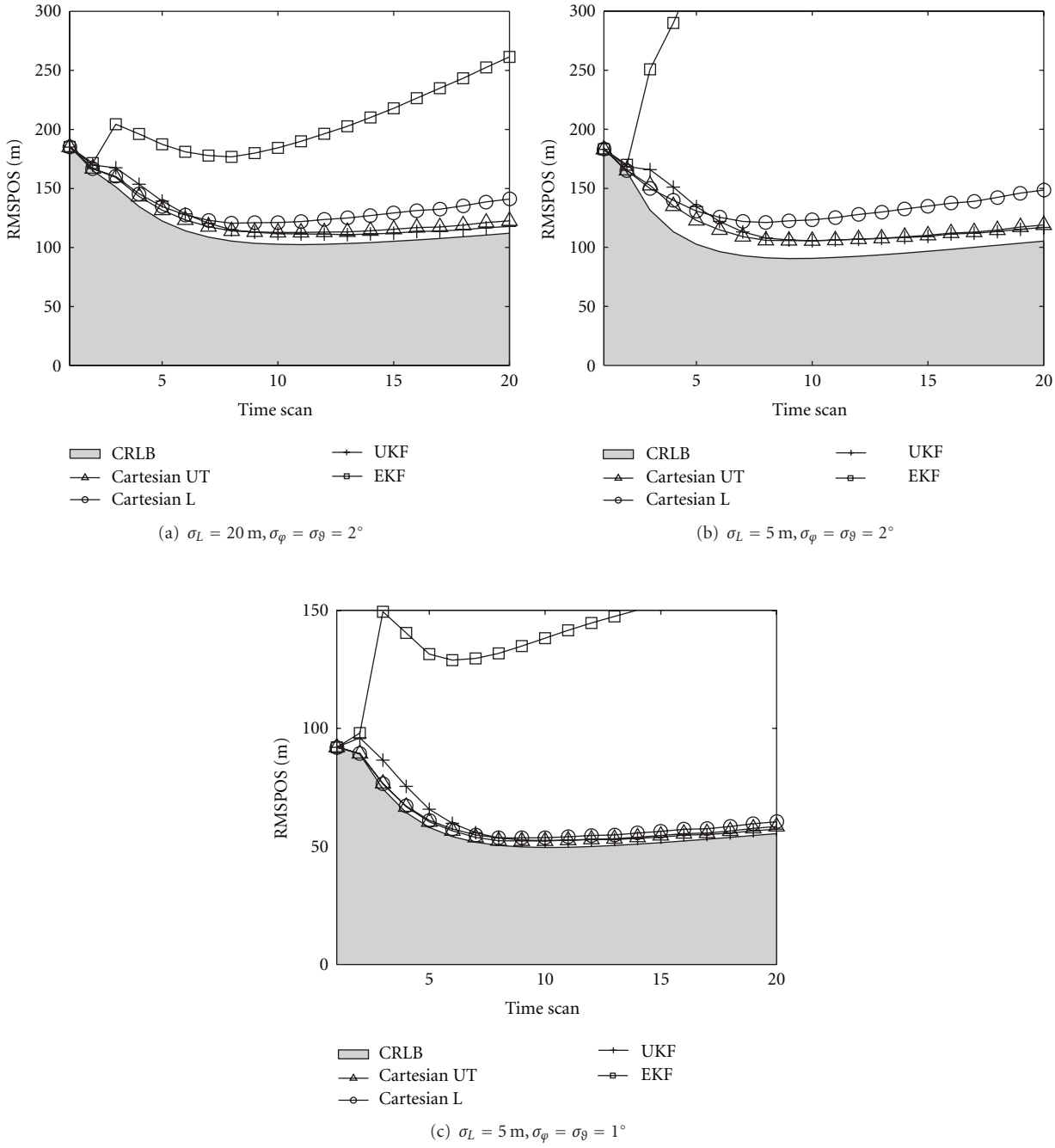

FIGURE 18: Comparison of different types of Kalman filters: In (a) the standard setting was used; (b) and (c) illustrate results for modifications in bearing and sensor precision. The EKF shows the worst tracking performance.

approximations of the transformation of measurements into Cartesian coordinates and reverse. In Figure 19(a), the grey dots denote Cartesian representatives when sampling from the (extended) artificial measurement vector $\mathbf{z}^{(a)}$. The solid and dashed line ellipses show the 3σ-gate of the approximated Gaussians generated by linearization or UT, respectively. In contrast, on the right-hand side (Figure 19(b)) the grey dots denote measurement representatives that is sampled from the extended state vector $\mathbf{x}_k^{(a)}$, whereas the uncertainty in the Cartesian is given by the CRLB. Again, solid and dashed line ellipses denote the approximation resulting from the linearization or UT method. For the standard scenario (not displayed here), both methods (UT and Linearization) deliver quite good approximations of the actual densities. The covariances given by the UT are slightly higher than of the linearization method. If we consider more accurate information of source and receiver position, the impact of the bearing uncertainty on the total localization error increases, see Figure 19(a). The shape of the samples (grey dots) diverges from an elliptic shape, thus

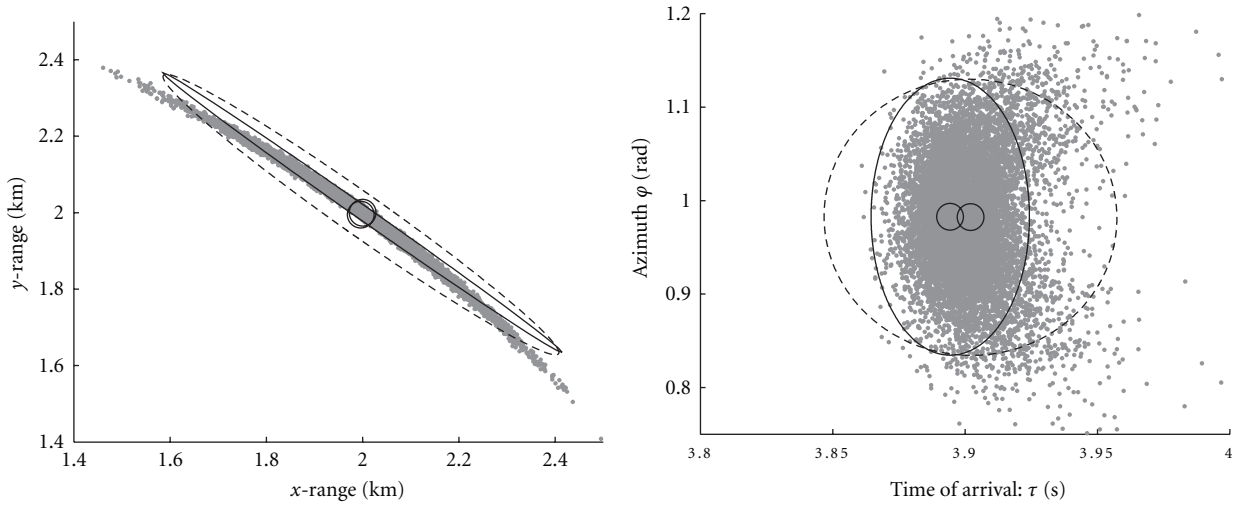

(a) Cartesian, $\sigma_L = 5\,\text{m}$ (b) Measurement, $\sigma_L = 5\,\text{m}$

Figure 19: Nonlinear transformations: (a) shows approximations of the transformation of measurements into Cartesian coordinates; (b) show results for the transformation of Cartesian estimates into measurement coordinates. Solid line ellipses correspond to linearization, dashed lines to UT, grey dots represent samples from the true density: for strong bearing dependencies both approximation techniques fail.

the approximation by a Gaussian fails. The approximation schemes (both UT and linearization) give unsatisfying results. However, the UT delivers larger covariances which seem to fit better and be more robust.

(c) *Dependency on the Time Interval.* In the prediction step of the KF, the state covariance matrix increases in dependency on the accuracy of the previous state estimate, the time between two consecutive pings and the maneuver modelling (not considered here). Thus, a low measurement update rate results in relatively large state covariance matrices, especially in the beginning when there is only poor knowledge about the target velocity. Thus, the information gained from the previous time scans is only poor. In comparison to that, the measurement provides a good localisation of the target for the current ping. During the EKF measurement update, the Jacobian is evaluated at the predicted target state (which is only a poor estimate of the current target state). Thus, linearization according to the Jacobian gives a poor approximation in the region, which is of actual interest.

In contrast, the covariance of the UKF is very large and compensates for approximation errors. Neither the approach UKF nor EKF will show optimal performance in such situations. The EKF may diverge or be biased, whereas the results of the UKF are degraded by large covariances. As shown in the tracking results, the UKF is more robust and recovers when the accuracy in the state estimate is improved after some pings.

(d) *Multistatic Fusion.* Referring to bistatic tracking performance, the two methods based on UT (Cartesian UT and UKF) are preferable and deliver robust tracking results. Generally, the results state approximation works best if the accuracy in the probability density that is to be transformed is high. This is so, if the accuracy in the estimated target state is poor compared to the accuracy in the measurement information (e.g., in the beginning due to the unknown target velocity), the Cartesian versions of the KF work best, since it uses transformation of the measurement information. Otherwise, if accuracy in track state is good (e.g., after maintaining the track for some pings) the UKF and EKF outperform the Cartesian L and Cartesian UT. This holds especially for multistatic tracking, which is demonstrated by numerical analysis of a multistatic scenario with two sources (placed at $(-2\,\text{km}, 0\,\text{km})^T$ and $(2\,\text{km}, 0\,\text{km})^T$) and one receiver (at $(0\,\text{km}, 0\,\text{km})^T$). The track state is sequentially updated according to the contact information of the different S/R pairs. Since data association is not a issue for these considerations the "AND" and "OR" fusion are to produce identical results. Figure 20 provides results for this scenario and the standard parameter settings. Figure 20(a) corresponds to a synchronous measurement update, that is, contact information of different S/R pairs are generated at the same time and the update rate is every $T = 60$ seconds. In Figure 20(b), we consider a asynchronous measurement update, the time between two consecutive pings of the same S/R pair is again $T = 60$ seconds, but with an offset of 30 s between different S/R pairs. All four methods deliver improved results compared to the case of a single S/R pair. The UKF proves again as robust and is also efficient (achieves the CRLB asymptotically) for the synchronous measurement update.

8.2.2. Sensitivity Studies of the MHT. The performance of the MHT depends on various parameters: it depends on the accuracy in measurement information, as well as on measurement false alarm rate and target manoeuvres. Generally, the MHT is known to be a powerful tool when faced with many false alarms inherent in multistatic sonar data. This issue is investigated in the next subsection. We will

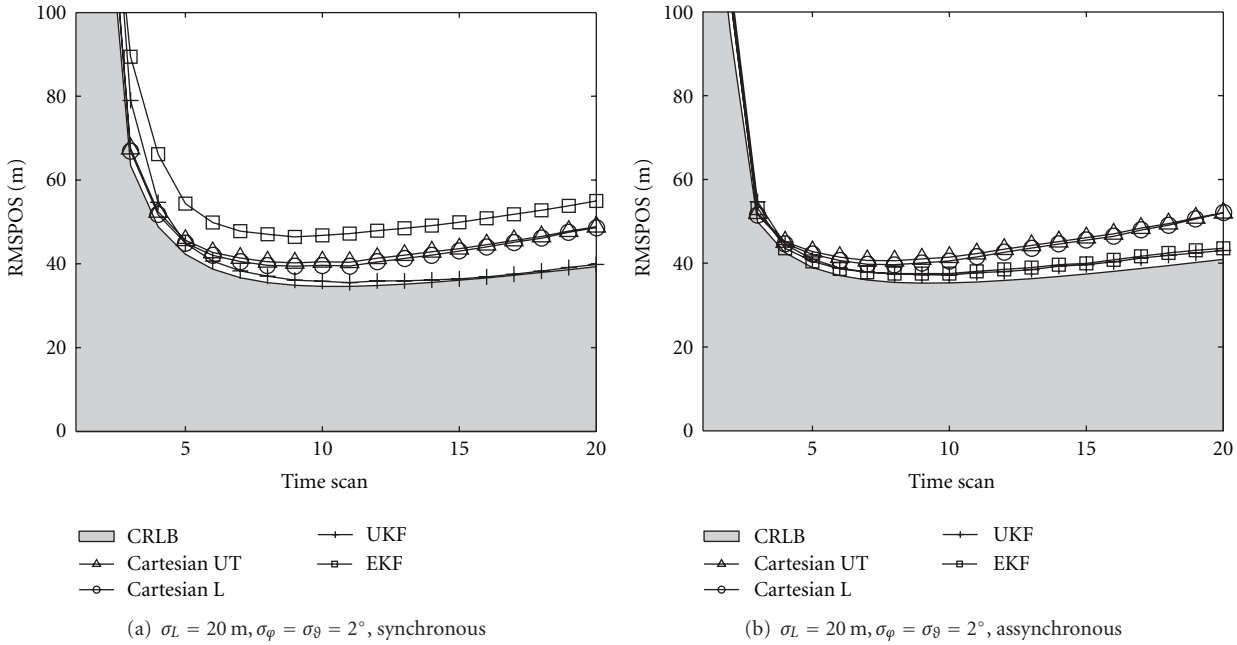

(a) $\sigma_L = 20\,\text{m}, \sigma_\varphi = \sigma_\vartheta = 2^\circ$, synchronous

(b) $\sigma_L = 20\,\text{m}, \sigma_\varphi = \sigma_\vartheta = 2^\circ$, assynchronous

Figure 20: Comparison of different types of Kalman filters: multistatic scenario with two sources and one receiver.

discuss the adaptive scan size of the MHT in the subsection after that.

(a) *Description of the Data Set.* For simulation, we follow the multistatic setup of SEABAR07 (one source, two receivers and one target) and simulate the target according to the specifications of the Run A01, see Figure 9(b). This provides the opportunity to statistically evaluate a realistic S/R receiver geometry combined with a manoeuvring target. For each S/R pair, we generate measurements according to $\sigma_\tau = 0.01$ and run 100 Monte Carlo runs for different values of σ_φ and false alarm rate (uncertainties in the environmental parameters are currently ignored). We limit this study to the simulation of FM contacts and no missing detections are considered. False alarms are generated uniformly in a 4 km $\times$ 7 km region around the target. We choose the values of DT and IT such that all simulated contacts (true contacts as well as false alarms) are considered for measurement update as well as track initiation. As measures of performance, we consider in this section the true data association probability and track continuation. For the true data association probability we count for true target contacts that are associated to the track in the strongest hypothesis of the MHT. Only measurements associated with extracted tracks are counted such that a long track extraction phase will display in worse performance. The track continuity is measured by counting for the pings in which a track is displayed by the MHT.

(b) *Results: MHT Performance for Different Rates of False Alarms and Measurement Accuracies.* Figure 21(a) shows results in terms of the true data association probability (in dependency on the azimuth accuracy and the false alarm rate) when processing measurements of the receiver RX2 only.

The performance of the MHT decreases with decreasing measurement accuracy and increasing number of false alarms. This is consistent with the expectations: Less accuracy in the track state results in an increasing size of the association gate. Thus, the probability to decide for a wrong data association increases. The same holds for an increasing false alarm rate. Processing measurements of both S/R pairs simultaneously (following the "AND" fusion strategy of FM contacts of RX2 and RX3) does result in good precision of the target state (exploiting triangulation gain) and does therefore improve the overall MHT performance. In the example considered before (when considering additional measurements of RX3), the probability of true association is 87%, 82%, and 69% for the high false alarm rate (i.e., 20 false alarms) and a measurement error in azimuth of $\sigma_\varphi = 1.5^\circ$, $\sigma_\varphi = 2^\circ$ and $\sigma_\varphi = 2.5^\circ$, respectively. Thus, the MHT can handle a higher false alarm rate, if measurements of both receivers are considered. Track continuity is generally better than the probability of true association, since due to the nature of the MHT the algorithm is able to regenerate from wrong or missed associations. Figure 21(b) shows (for the single S/R pair case) both measures of tracking performance plotted versus the ping number for $\sigma_\varphi = 2.5^\circ$ and 20 false alarms per ping. When considering measurements of both S/R pairs, the corresponding results are visualized in Figure 21 for small (c) and large (d) azimuth errors. For small azimuth uncertainty, the track is continuously maintained after track extraction (track continuity is 100%). We observe some failure in measurement association (especially during the target manoeuvres) from that the algorithm can recover. Performance is worse for large measurement inaccuracies,

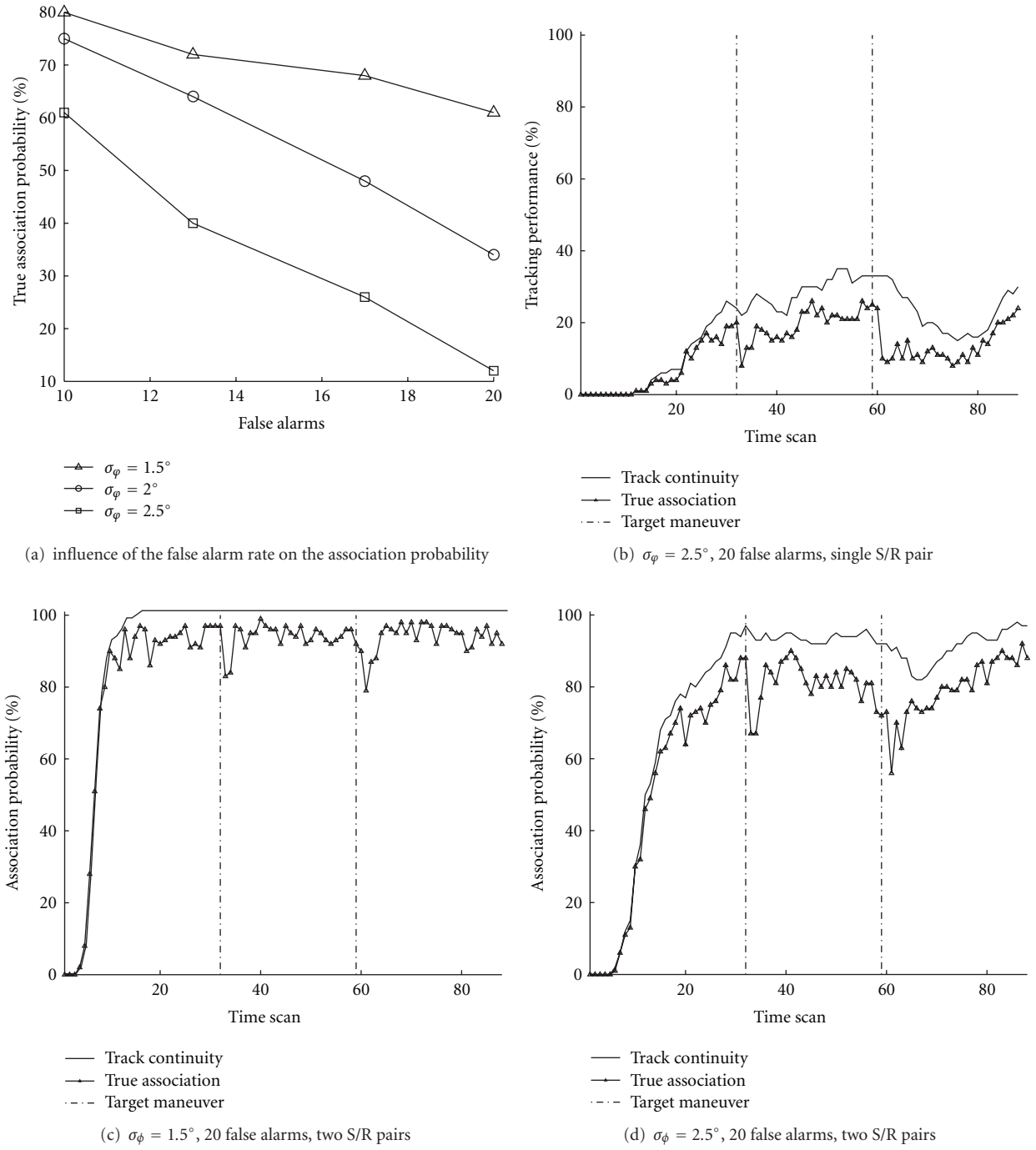

(a) influence of the false alarm rate on the association probability

(b) $\sigma_\varphi = 2.5°$, 20 false alarms, single S/R pair

(c) $\sigma_\phi = 1.5°$, 20 false alarms, two S/R pairs

(d) $\sigma_\phi = 2.5°$, 20 false alarms, two S/R pairs

Figure 21: Impact of the number of false alarms and azimuth accuracy on tracking performance. In (a) and (b) only one S/R pair in (c) and (d) two S/R pairs are considered.

but we still observe a probability of 90% to track the target. After the second manoeuvre the probability decreases for a short period, some tracks seem to get lost during the manoeuvre. Comparing Figures 21(b) and 21(d), we note a significant improvement due to the consideration of a second receiver.

For all results, we observe a comparable and very low false track rate that is no further specified here.

9. Summary

When designing an algorithm for tracking of multistatic sonar data, three major questions have to be answered:

(1) handling the nonlinear measurement information,

(2) choice of fusion architecture,

(3) fusing information of CW and FM (accounting for the specific characteristics of the two different wave forms).

The paper discusses several solutions fitting into a MHT structure. Extending the MHT strategy to incorporate deterministic and probabilistic a priori knowledge seems to be a viable way towards a robust, precise, and real-time capable multistatic tracking algorithm.

(at 1.) Due to the nonlinearity in the measurement model, approximation techniques are necessary to apply sequential target tracking to data from a bistatic sonar system. In this paper, we have implemented two approximation techniques, (based on linearization and unscented transform (UT)), and studied their performance when mapping bistatic data to the Cartesian system. Tracking is possible for both techniques in the Cartesian system (Cartesian L and Cartesian UT). We compared their performance based on simulated data, relative to the CRLB. Comparing the approximation techniques, we found that linearization tends to underestimate the actual errors whilst the UT tends to overestimate. Referring to tracking performance, the Cartesian UT seems to be preferable. Also, the extended Kalman filter (EKF) [5] and unscented Kalman Filer (UKF) [4] can be adapted to account for the probabilistic features of the bistatic sonar measurement. In total, there are four different tracking methods. Due to our analysis, the EKF seems to be not recommended in most of the scenarios considered here. In literature, the iterated EKF [20] is proposed to improve robustness of the EKF; alternatively, we propose a combination of Cartesian L (during the first pings) and EKF. Tested by detailed simulation, the UKF method was chosen to be incorporated into the structure of a MHT tracking algorithm and was evaluated by applying them to real data sets. We found the MHT to be capable of extracting and maintaining the target in three experimental data sets and showed that by correct modelling of the deterministic features of the underwater sound channel a bias in the tracking result can be reduced.

(at 2.) To exploit the advantages of a multistatic setup an appropriate fusion strategy must be developed to process measurements of different source and receiver pairs. We found (and therefore confirm the findings in [21]) that the "AND" fusion strategy outperforms the "OR" fusion strategy in regions of overlapping sensor coverage. But, the "AND" fusion strategy is sensitive to an appropriate description of the likelihood function. Sonar performance modelling [22] shows that correct modelling of the probability of detection of each source/receiver pair and for each hypothetic track is therefore of particular importance. We developed an approach to incorporate sonar performance modelling in the framework of automatic sequential tracking techniques and showed with experimental sonar data that they are able to improve robustness of the "AND" fusion strategy.

(at 3.) Based on an algorithm from ground moving target tracking, we implemented a strategy to fuse contact information of the FM and CW signal. We found the algorithm to be capable of the application to multistatic sonar data and noted a significant reduction of the false track rate due to the fusion of FM and CW contacts. Moreover, the algorithm is able to process larger number of false alarms when measurements of the FM and CW signal are fused. The fusion strategies have been evaluated by applying them to experimental sonar data.

10. Conclusion

It is possible to implement in an MHT framework an automatic data fusion algorithm that exploits all advantages of the multistatic setup. As the multistatic setup is mandatory in difficult measurement scenarios, our implementation allows to provide the operator with accurate and simplified true target extraction by a drastic decrease in the number of false alarms.

The analysis of simulated and real data sets showed that the advantages of multistatic sonar can only be exploited if the measurement model is correct. That is, we need to interpret correctly the measurement information and the events of false alarms and missed detections. However, the precision of modelling knowledge for underwater sound is limited by the stochastic fluctuations/uncertainties. Therefore, in order to provide a robust algorithm it is important not to overestimate the accuracy of the modelling: "Be honest with your tracker!".

Appendix

In this subsection, we describe used measures of performance: Average Estimation Error, Cramér Rao Lower Bound and Consistency.

(a) *Average Estimation Error.* The root-mean-square error of the position estimate (RMSPOS), is an absolute error measure and direct performance criterion. It is averaged over all simulation runs. The RMSPOS error from N Monte Carlo runs is

$$\mathrm{RMSPOS}(\mathbf{x}_k) = \sqrt{\frac{1}{N}\sum_{i=1}^{N} \left| \widetilde{\mathbf{x}}_{k,i} - \mathbf{x}_k \right|^2}, \tag{A.1}$$

where $\widetilde{\mathbf{x}}_{k,i}$ is the position estimate at run i and $\mathbf{x}_k$ the position of the truth.

(b) *Cramér Rao Lower Bound.* Since we consider nonlinear measurements and additive white Gaussian noise $\mathbf{w}$, the Cramér Rao lower bound (CRLB) with respect to the likelihood function $\Lambda(\mathbf{x}^{(a)}) = p(\mathbf{z} \mid \mathbf{x}^{(a)})$ can be derived in a standard way. The general calculation of the Fisher information matrix can be replaced by a more specialized formula

$$\begin{aligned} \mathbf{J}_0 &= \mathbf{E}\left\{ \left[\nabla_{\mathbf{x}^{(a)}} \log \Lambda\left(\mathbf{x}^{(a)}\right) \right] \left[\nabla_{\mathbf{x}^{(a)}} \log \Lambda\left(\mathbf{x}^{(a)}\right) \right]^T \right\} \\ &= \frac{\partial h}{\partial \mathbf{x}^{(a)}} \mathrm{Cov}(\mathbf{w})^{-1} \left(\frac{\partial h}{\partial \mathbf{x}^{(a)}} \right)^T. \end{aligned} \tag{A.2}$$

In our application, we consider the 9-dimensional state vector $\mathbf{x}^{(a)} = (\mathbf{x}; \mathbf{a})$ (see Section 6.2) versus the 2-dimensional measurement vector $\mathbf{z}$, so the matrix $\mathbf{J}_0$ will not be invertible. This shows that we cannot estimate the full state vector $\mathbf{x}^{(a)}$ without additional assumptions. As information is additive, these additional assumptions in the form of a prior distribution in $\mathbf{a}$, can be added to the Fisher information matrix [23]

$$\mathbf{J} = \mathbf{J}_0 + \mathbf{J}_P, \tag{A.3}$$

where $\mathbf{J}_P$ is the Fisher information of the prior

$$\mathbf{J}_P = \begin{bmatrix} 0 & 0 \\ 0 & \mathbf{C}_a^{-1} \end{bmatrix}. \tag{A.4}$$

The CRLB results from the Fischer information by inversion. To compare the CRLB with the corresponding RMSPOS we use the rooted trace of the 2D position matrix, that is, $\sqrt{\mathrm{CRLB}(1,1) + \mathrm{CRLB}(2,2)}$.

(c) *Consistency.* Filter consistency is usually measured using the normalized (state) estimation error squared (NEES), defined as

$$\epsilon = (\hat{\mathbf{x}} - \mathbf{x})^T \hat{\mathbf{P}}^{-1} (\hat{\mathbf{x}} - \mathbf{x}), \tag{A.5}$$

where $\hat{\mathbf{x}}$ and $\hat{\mathbf{P}}$ are expectation and covariance of the estimate that are compared to the truth $\mathbf{x}$. ϵ should be chi-square distributed with $\eta_{\mathbf{x}}$ degrees of freedom, if the filter is consistent. In Monte Carlo simulations that provide N independent samples ϵ_i, $i = 1, \ldots, N$, the average NEES is

$$\overline{\epsilon} = \frac{1}{N} \sum_{i=1}^{N} \epsilon_i. \tag{A.6}$$

It has to be tested whether $N\overline{\epsilon}$ is chi-square distributed with $N\eta_{\mathbf{x}}$ degrees of freedom. This hypothesis is accepted, if $N\overline{\epsilon}$ is in the appropriate acceptance region.

Acknowledgments

This work was made possible through collaboration between NURC, a NATO Research Centre and Fraunhofer FKIE (DEU). The authors would like to thank W. Koch, M. Ulmke, D. Grimmet, O. Eroglu, E. Baglioni, K. Seget, and the members of the ISIF MSTWG [24] for discussions and support. This paper was presented in part at the FUSION, Cologne, Germany, July 2008 [19], and OCEANS, Bremen, Germany, May 2009 [25] and the GI Jahrestagung, Lübeck, Germany, October 2009 [26].

References

[1] Y. Bar-Shalom and X.-R. Li, *Multitarget-Multisensor Tracking: Application and Advances*, Artech House Radar Libary, 1995.

[2] R. Klemm and W. Koch, "Ground target tracking with STAP radar: selected tracking aspects," in *Principles of Space Time Adaptive Processing*, 2002.

[3] H. Cox, "Fundamentals of active sonar," in *Underwater Acoustic Data Processing*, pp. 3–24, 1989.

[4] S. J. Julier and J. K. Uhlmann, "Unscented filtering and nonlinear estimation," *Proceedings of the IEEE*, vol. 92, no. 3, pp. 401–422, 2004.

[5] W. Denham and S. Pines, "Sequential estimation when measurement function nonlinearity is comparable to measurement error," *AIAA Journal*, vol. 4, no. 4, pp. 1071–1076, 1966.

[6] S. Coraluppi, "Multistatic sonar localization," *IEEE Journal of Oceanic Engineering*, vol. 31, no. 4, pp. 964–974, 2006.

[7] R. Been, S. Jespers, S. Coraluppi, C. Carthel, C. Strode, and A. Vermeij, "Multistatic sonar: a road to a maritime network enabled capability," in *Proceedings of Undersea Defence Technology Europe*, Naples, Italy, June 2007.

[8] D. T. Hughes, R. Been, and A. Vermeij, "Heterogenous underwater networks for ASW: technology and techniques," in *Maritime Systems and Technology*, Genova, Italy, 2008.

[9] C. R. Berger, M. Daun, and W. Koch, "Low complexity track initialization from a small set of non-invertible measurements," *EURASIP Journal on Advances in Signal Processing*, vol. 2008, Article ID 756414, 2008.

[10] N. J. Willis, *Bistatic Radar*, SciTech, 2007.

[11] S. Blackman and R. Popoli, *Design and Analysis of Modern Tracking Systems*, Artech House, Boston, Mass, USA, 1999.

[12] Y. Bar-Shalom, X. R. Li, and T. Kirubarajan, *Estimation with Application to Tracking and Navigation*, John Wiley & Sons, New York, NY, USA, 2001.

[13] W. Koch, J. Koller, and M. Ulmke, "Ground target tracking and road map extraction," *ISPRS Journal of Photogrammetry and Remote Sensing*, vol. 61, no. 3-4, pp. 197–208, 2006.

[14] R. J. Urick, *Principles of Underwater Sound*, McGraw-Hill Education, New York, NY, USA, 2nd edition, 1976.

[15] M. Daun, W. Koch, and R. Klemm, "Tracking of ground targets with bistatic airborne radar," in *Proceedings of IEEE Radar Conference (RADAR '08)*, pp. 1–6, May 2008.

[16] W. Koch, "Fixed-interval retrodiction approach to Bayesian IMM-MHT for maneuvering multiple targets," *IEEE Transactions on Aerospace and Electronic Systems*, vol. 36, no. 1, pp. 2–14, 2000.

[17] D. Grimmet, "Data set A01 (target strength amendment) and Data set A56 (time synchronization)," private communication.

[18] S. Coraluppi, D. Grimmett, and P. de Theije, "Benchmark evaluation of multistatic trackers," in *Proceedings of the 9th International Conference on Information Fusion*, July 2006.

[19] M. Daun and F. Ehlers, "Multistatic multihypothesis tracking: environmentally adaptive and high-precision state estimates," in *Proceedings of the 11th International Conference on Information Fusion*, pp. 1–8, June 2008.

[20] T. Lefebvre, H. Bruyninckx, and J. de Schutter, "Kalman filters for non-linear systems: a comparison of performance," *International Journal of Control*, vol. 77, no. 7, pp. 639–653, 2004.

[21] O. Gerard, S. Coraluppi, C. Carthel, and D. Grimmett, "Benchmark analysis of NURC multistatic tracking capability," in *Proceedings of the 9th International Conference on Information Fusion*, July 2006.

[22] A. Wathelet, C. Strode, and A. Vermeij, "Simulating multistatic asw operations with the multistatic tactical planning aid (mstpa) for tactics development," in *NATO RTO Modelling and Simulation Group Conference on 'Improving M&S Interoperability, Reuse and Efficiency in Support of Current and Future Forces'*, pp. 1–10, October 2007.

[23] H. van Trees, *Detection, Estimation, and Modulation Theory*, John Wiley & Sons, New York, NY, USA, 1st edition, 1968.

[24] "International Society of Information Fusion," http://www.isif.org/.

[25] F. Ehlers, M. Daun, and M. Ulmke, "System design and fusion techniques for multistatic active sonar," in *Proceedings of OCEANS Conference*, pp. 1–10, May 2009.

[26] M. Daun and F. Ehlers, "Tracking algorithms for bistatic sonar systems," in *INFORMATIK' 09 - Jahrestagung der Gesellschaft fuer Informatik e.V. (GI) 4th German Workshop Sensor Data Fusion (SDF'09)*, pp. 2283–2295, Lübeck, Germany, October 2009.